arXiv:1812.07773v1 [physics.space-ph] 19 Dec 2018

Dynamics in first-order mean motion resonances: analytical study of a simple model with stochastic behaviour

S. Efimov · V. Sidorenko

Abstract We examine a 2DOF Hamiltonian system, which arises in study of first-order mean motion resonance in spatial circular restricted three-body problem "star-planet-asteroid", and point out some mechanisms of chaos generation. Phase variables of the considered system are subdivided into fast and slow ones: one of the fast variables can be interpreted as resonant angle, while the slow variables are parameters characterizing the shape and orientation of the asteroid's orbit. Averaging over the fast motion is applied to obtain evolution equations which describe the long-term behavior of the slow variables. These equations allowed us to provide a comprehensive classification of the slow variables' evolution paths. The bifurcation diagram showing changes in the topological structure of the phase portraits is constructed and bifurcation values of Hamiltonian are calculated. Finally, we study properties of the chaos emerging in the system.

Keywords Hamiltonian system · averaging method · mean motion resonance · chaotic dynamics

1 Introduction

The model system which will be considered below arises in studies of first-order mean motion resonances (MMR) in restricted three-body problem (R3BP) "star-planet-asteroid". If asteroid makes $p \in N$ revolutions around the star in the same amount of time in which the planet makes $p+1$ revolutions, there is an *exterior* resonance of the first-order denoted as $p:(p+1)$. The term exterior refers to the fact that in this case the asteroid's semi-major axis is larger than semi-major axis of the planet. The *interior* MMR $(p+1):p$ takes place when asteroid makes $p+1$ revolutions during the time in which planet makes p. The first-order MMRs are quite common and, therefore, intensively studied by many specialists. The related bibliography is given in Gallardo (2018) and Nesvorny et al. (2002). In particular, much effort has been spent to reveal why $2:1$ resonance with Jupiter corresponds to one of the largest gaps in the main asteroid belt (so-called Hecuba gaps), whereas $3:2$ MMR resonance is populated by numerous objects of Hilda group, and it is also very likely, that Thule group of objects in $4:3$ MMR is rather large (Broz

S. Efimov
Moscow Institute of Physics and Technology
9 Institutskiy per., Dolgoprudny, Moscow Region, 141701, Russian Federation
E-mail: efimov.ss@phystech.edu

V. Sidorenko
Keldysh Institute of Applied Mathematics
Russian Academy of Sciences,
Miusskaya Sq., 4, 125047 Moscow, Russian Federation
and

Moscow Institute of Physics and Technology
9 Institutskiy per., Dolgoprudny, Moscow Region, 141701, Russian Federation

and Vokrouhlicky 2008; Henrard 1996; Lemaitre and Henrard 1990). The discoveries of trans-Neptunian objects made it urgent to study the exterior resonances with Neptune: *twotino* (MMR 1 : 2) and *plutino* (MMR 2 : 3) form big subpopulations in the Kuiper belt (Li et al. 2014a,b; Nesvorny and Roig 2000, 2001).

It is possible to construct a model of dynamics in first-order MMR, taking into account only the leading terms in the Fourier series expansion of disturbing function (Sessin and Ferraz-Mello 1984; Wisdom 1986; Gerasimov and Mushailov 1990). However, studies of planar R3BP (Beaugé 1994; Jancart et al. 2002) revealed, that some important characteristics of first-order MMRs are reproduced only when the second-order Fourier terms are accounted for. In this paper we concentrate our attention on that part of a phase space, where eccentricities and inclinations are in relation $e \ll i \ll 1$ (this, in some sense, is a case opposite to the planar problem, for which the relation is $e > i = 0$). We intend to demonstrate, that in non-planar case second-order terms are no less important, as they make a model essentially stochastic. In contrast, the first-order models are proven to be integrable (Sessin and Ferraz-Mello 1984), and thus cannot reproduce chaotic dynamics found in multiple numerical studies of first-order resonances (Wisdom and Sussman 1988; Giffen 1973; Winter and Murray 1997a,b; Wisdom 1987),

There are different mechanisms for generating chaos in the dynamics of celestial bodies (Holmes 1990; Lissauer 1999; Morbidelli 2002). Presence of MMR may lead to the so-called adiabatic chaos (Wisdom 1985), which is caused, roughly speaking, by small quasi-random jumps between regular phase trajectories in certain parts of the phase space, where adiabatic approximation is violated. Applying systematically Wisdom's ideas to study of MMRs (Sidorenko 2006; Sidorenko et al. 2014; Sidorenko 2018), we found that adiabatic chaos often coexists with the quasi-probabilistic transitions between specific phase regions. Both phenomena occur in that part of the phase space, where the "pendulum" or first-order Second Fundamental Model for Resonance (Henrard and Lamaitre 1983) approximations fail, because the first harmonic in the disturbing function Fourier series is not dominant. The goal of this paper is to carry out a comprehensive analysis of the introduced second-order model and investigate described mechanisms of chaotization, which, in our opinion, have not received proper attention in the past.

The paper is organized as follows. In Section 2 the model Hamiltonian system, which has a structure of slow-fast system, is introduced. In Section 3 the fast subsystem is studied. Equations of motion for slow subsystem are constructed in Section 4 and their solutions are analyzed in Section 5. Section 6 is devoted to different chaotic effects present in the discussed model. In Section 7 numerical evidence for existence of described phenomena is shown. The results are summarized in the last section. In Appendix A we reveal how the proposed model was derived. Details of the averaging procedure are elucidated in Appendix B.

2 Model Hamiltonian system

We are dealing with 2DOF Hamiltonian systems with specific symplectic structure:

$$\begin{aligned} \frac{d\varphi}{d\tau} &= \frac{\partial \Xi}{\partial \Phi}, \qquad \frac{d\Phi}{d\tau} = -\frac{\partial \Xi}{\partial \varphi}, \\ \frac{dx}{d\tau} &= \varepsilon \frac{\partial \Xi}{\partial y}, \qquad \frac{dy}{d\tau} = -\varepsilon \frac{\partial \Xi}{\partial x}. \end{aligned} \tag{1}$$

The Hamiltonian Ξ in (1) is expressed by

$$\Xi(x, y, \varphi, \Phi) = \frac{\Phi^2}{2} + W(x, y, \varphi), \; W(x, y, \varphi) = x \cos\varphi + y \sin\varphi + \cos 2\varphi. \tag{2}$$

Appendix A describes in detail how the system (1)-(2) arises in studies of first-order MMR in three-dimensional R3BP. Here we only note that

$$\varepsilon \sim \mu^{1/2}, \quad x \propto e \cos\omega, \quad y \propto -e \sin\omega,$$

where $\mu \ll 1$ is the fraction of the planet's mass in the total mass of the system, e and ω denote the eccentricity and the argument of pericenter of asteroid's osculating orbit respectively. Further ε is treated as a small parameter of the problem. Since in general variables φ, Φ, x, y vary with different rates

($d\varphi/d\tau, d\Phi/d\tau \sim 1$, while $dx/d\tau, dy/d\tau \sim \varepsilon \ll 1$), we can distinguish in (1) *fast* subsystem (described by the first line of equations) and *slow* subsystem (the second line).

In limiting case $\varepsilon = 0$ equations of fast subsystem coincide with equations of motion for particle with unit mass in a field with potential $W(x, y, \varphi)$, where x and y are treated as parameters. Let

$$\varphi(\tau, x, y, \xi), \quad \Phi(\tau, x, y, \xi) \tag{3}$$

be a solution of fast subsystem with fixed values of x, y, and value ξ of Hamiltonian Ξ, which is the first integral of system (1). In general the resonant angle φ in (3) can *librate* between two constant values or change monotonously through the whole interval $[0, 2\pi)$, i.e. *circulate*. In either case

$$\varphi(\tau + T, x, y, \xi) = \varphi(\tau, x, y, \xi) \bmod (2\pi)\,,$$

where $T(x, y, \xi)$ is a period of the solution (3).

Because fast variables vary much faster then the slow ones, the right-hand sides in differential equations of slow subsystem in (1) can be replaced by their average values along the solution (3). This yields the *evolution equations*, which describe secular variations of x and y in closed form:

$$\frac{dx}{d\tau} = \varepsilon \left\langle \frac{\partial \Xi}{\partial y} \right\rangle, \ \frac{dy}{d\tau} = -\varepsilon \left\langle \frac{\partial \Xi}{\partial x} \right\rangle. \tag{4}$$

Here

$$\langle \Lambda \rangle = \frac{1}{T(x, y, \xi)} \int\limits_0^{T(x,y,\xi)} \Lambda(x, y, \varphi(\tau, x, y, \xi)) d\tau. \tag{5}$$

The solution (3) has an action integral:

$$J(x, y, \xi) = \frac{1}{2\pi} \int\limits_0^{T(x,y,\xi)} \Phi^2(\tau, x, y, \xi) d\tau. \tag{6}$$

For $\varepsilon \neq 0$ function $J(x, y, \xi)$ becomes an adiabatic invariant of slow-fast system (1). For a fixed ξ trajectories of averaged equations (4) on a phase plane (x, y) go along the lines with constant values of J. This allows to classify evolution equations (4) as adiabatic approximation (Neishtadt 1987a; Wisdom 1985).

In the next Sections we go through all the steps in construction of evolution equations via described approach and analyze in detail the behaviour of slow variables on different levels of Hamiltonian $\Xi = \xi$.

3 Properties of fast subsystem's solutions for different values of slow variables (limiting case $\varepsilon = 0$)

3.1 Partition of the plane (x, y) based on the number of librating solutions

Because the variables x and y change very slowly (1), they can be treated as constant parameters, when considering the motion of the fast subsystem. Then the potential W is just a "two-harmonic" function of φ defined on circle S^1, and the motion in such potential can be described in terms of elliptic functions.

There are different types of motion depending on the Hamiltonian level ξ at which it occurs (Fig. 1). For us it is important, that for some values of x and y two different librating solutions can exist on the same ξ level (Fig. 1c). This situation can take place when $W(\varphi)$ has four extrema on S^1.

A necessary condition for extremum $\partial W/\partial \varphi = 0$ after the replacement $\lambda = \tan(\varphi/2)$ yields

$$y\lambda^4 + 2(x + 4)\lambda^3 + 2(x - 4)\lambda - y = 0. \tag{7}$$

Let $\mathcal{A}$ denote a region on the plane (x, y), in which $W(\varphi)$ has four extrema. The equation (7) has four real roots inside this region and only two outside. Thus on the border of the region $\mathcal{A}$ the number of unique

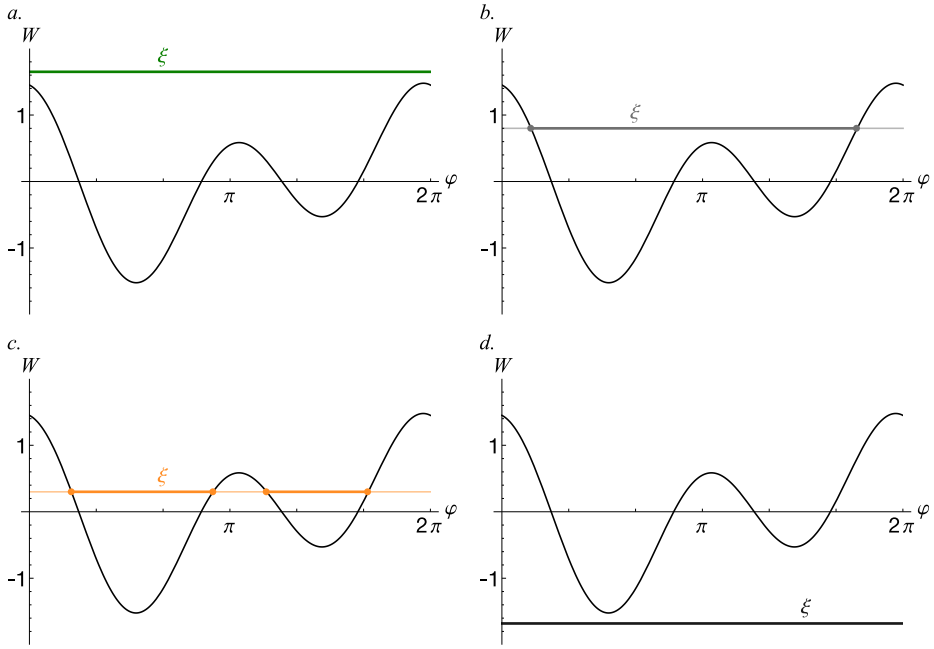


Fig. 1 Levels ξ of Hamiltonian Ξ corresponding to different types of fast subsystem's motion: a. circulation, b. libration, c. two coexisting librating solutions, d. the motion is impossible

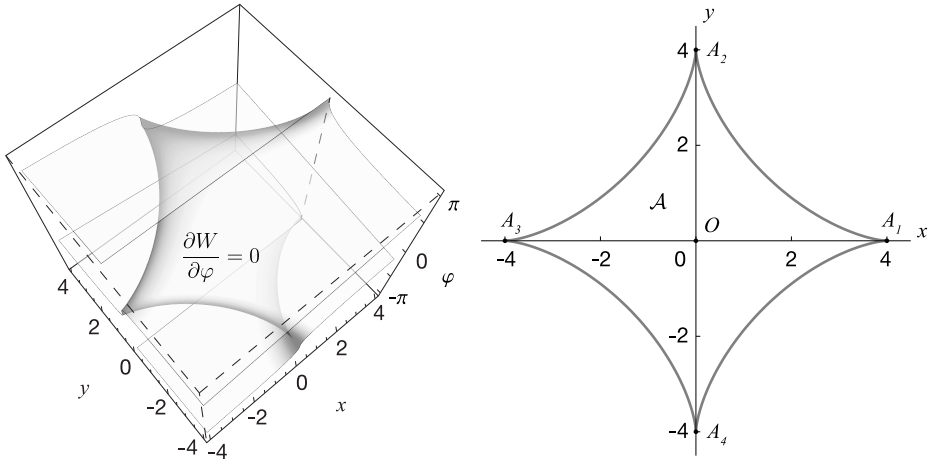


Fig. 2 Extremal surface of potential $W(x, y, \varphi)$ (left), and astroid bounding the region $\mathcal{A}$, where W has four extrema as a function of φ on S^1 (right). $A_1, \ldots, A_4$ – astroid's cusps

real roots is 3 (with the exception of finite number of points in which there is only one unique real root) and the discriminant of (7) is equal to zero. Therefore the equation for the border of the region $\mathcal{A}$ is

$$x^6 + 3x^4y^2 - 48x^4 + 3x^2y^4 + 336x^2y^2 + 768x^2 + y^6 - 48y^4 + 768y^2 - 4096 = 0. \tag{8}$$

By collecting the parts of this equation into perfect cube (8) is transformed to canonical algebraic equation of astroid (Fig. 2):

$$\left(x^2 + y^2 - 4^2\right)^3 + 27 \cdot 4^2x^2y^2 = 0. \tag{9}$$

Which can be further reduced to

$$x^{2/3} + y^{2/3} = 4^{2/3}. \tag{10}$$

It is convenient to use this astroid for the reference on the phase plane (x, y).

3.2 Critical curve partitioning the plane (x, y) into regions with different types of fast subsystem' motion

Let us introduce the notations $W_{min}(x, y)$ and $W_{max}(x, y)$ for global minimum and maximum of function W on S^1 for given values of slow variables. If $(x, y) \in \mathcal{A}$, then W has the second pair of minimum and maximum, which we shall denote $W^*_{min}(x, y)$ and $W^*_{max}(x, y)$ respectively. Using these auxiliary functions, we can partition the (x, y) plane for a given ξ into different regions based on the type of fast subsystem's motion:

$$
\begin{aligned}
Q_0 &= \{(x,y) \ \mid \xi < W_{min}\}, \\
Q_1 &= \big\{(x,y) \notin \mathcal{A} \ \big| \ \xi \in \big(W_{min}, W_{max}\big)\big\} \bigcup \\
&\qquad \big\{(x,y) \in \mathcal{A} \ \big| \ \xi \in \big(W_{min}, W_{max}\big) \setminus \big(W^*_{min}, W^*_{max}\big)\big\}, \\
Q_2 &= \big\{(x,y) \in \mathcal{A} \ \big| \ \xi \in \big(W^*_{min}, W^*_{max}\big)\big\}, \\
Q_3 &= \{(x,y) \ \mid \xi > W_{max}\}.
\end{aligned}
$$

The region $Q_0(\xi)$ will be called a *forbidden region*, because inside of it $\Xi < \xi$ for any values of fast variables and fast subsystem has no solutions (Fig. 1d). Region $Q_1(\xi)$ is the region with the single librating solution (Fig. 1b), $Q_2(\xi)$ is the region with two librating solutions at given level ξ (Fig. 1c), and finally the region $Q_3(\xi)$ is where fast subsystem's solution circulates (Fig. 1a). Illustrations for regions $Q_0(\xi), \ldots, Q_3(\xi)$ will follow.

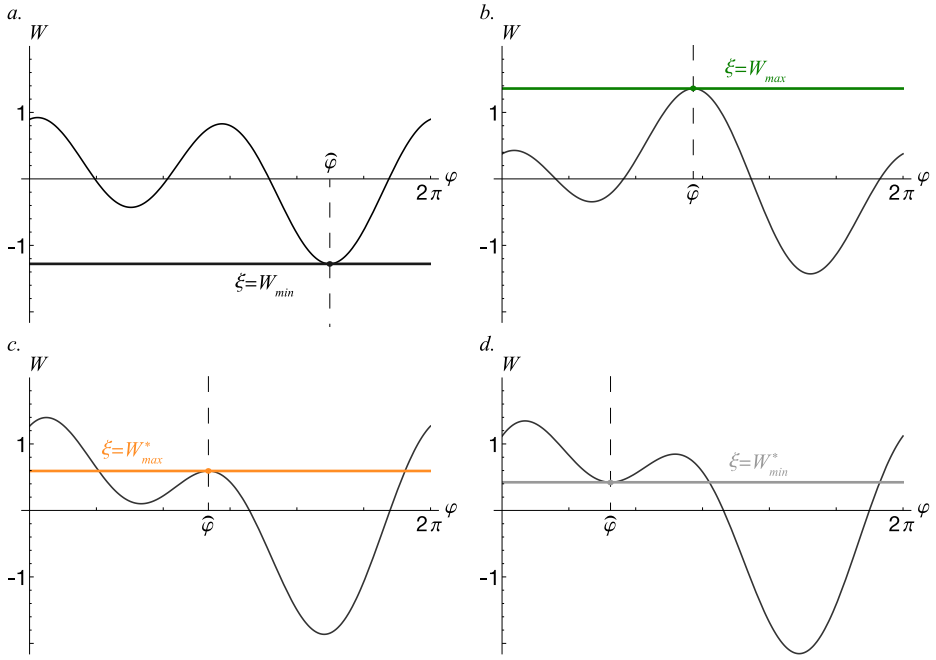


Fig. 3 Tangency of Hamiltonian level ξ and different extrema of $W(\varphi)$, which occurs on the borders of regions $Q_0(\xi), \ldots, Q_3(\xi)$

Before that let us consider a border $\Gamma(\xi)$ between these regions. In every point of the border value of W is equal to ξ in one of its critical points (cf. Figures 1 and 3), which is why we shall call $\Gamma(\xi)$ a *critical curve*. After replacement $\lambda = \tan(\varphi/2)$ the equation $W(\varphi) = \xi$ transforms into algebraic equation:

$$
(1 - \xi - x)\lambda^4 + 2y\lambda^3 - 2(\xi + 3)\lambda^2 + 2y\lambda + (x + 1 - \xi) = 0. \tag{11}
$$

As Figure 3 demonstrates, the point (x, y) lies on the critical curve when equation (11) have at least one multiple real root, which is equivalent to discriminant of (11) being equal to zero:

$$\begin{aligned} D(x,y,\xi) = 64\xi^4 - 128\xi^2 - x^6 + \xi^2 x^4 - 18\xi x^4 - 3x^4y^2 - 15x^4 + \\ + 16\xi^3 x^2 - 80\xi^2 x^2 - 144\xi x^2 - 3x^2y^4 + 2\xi^2 x^2 y^2 + 78x^2y^2 - 48x^2 - \\ - y^6 + \xi^2 y^4 + 18\xi y^4 - 15y^4 - 16\xi^3 y^2 - 80\xi^2 y^2 + 144\xi y^2 - 48y^2 + 64 = 0. \end{aligned} \quad (12)$$

Thus in the regions $Q_0(\xi)$, $Q_2(\xi)$, $Q_3(\xi)$ the discriminant $D(x, y, \xi) > 0$, while $D(x, y, \xi) < 0$ in $Q_1(\xi)$, and $D(x, y, \xi) = 0$ on the critical curve $\Gamma(\xi)$. Figure 4 depicts $\Gamma(\xi)$ on the plane of slow variables for different values of ξ. At $|\,\xi\,| < 3$ critical curve have cusps, which lie on astroid (10). Additionally this curve may have points of self-intersection. If $-3 < \xi < -1$, the curve intersects itself on axis x, with the x coordinates of self-intersection points being defined by equation

$$x^2 + 8(\xi + 1) = 0.$$

If $1 < \xi < 3$, points of self-intersection lie on y axis, and their y coordinates are defined by equation

$$y^2 - 8(\xi - 1) = 0.$$

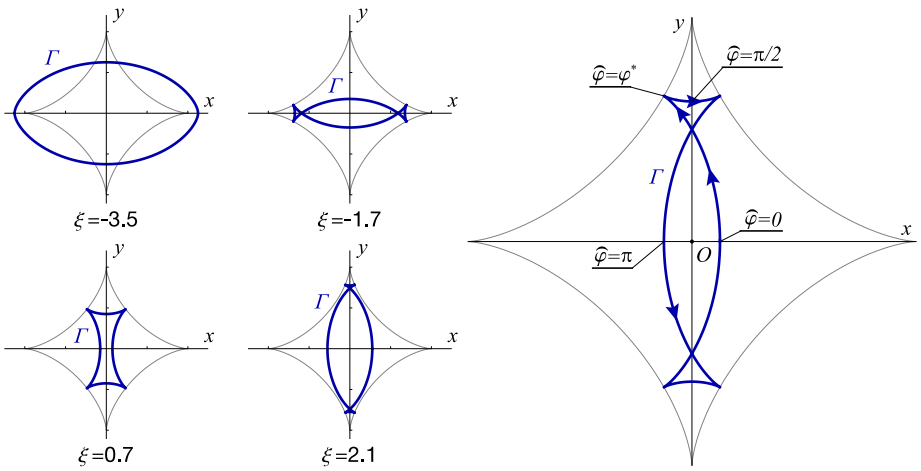


Fig. 4 Critical curve $\Gamma(\xi)$: shape of the curve for different ξ values (left), and parametrization of the curve by $\widehat{\varphi}$ with arrows showing the direction in which the parameter increases (right)

The critical curve allows a parametrization

$$\Gamma(\xi) = \left\{ x = \cos\widehat{\varphi}(\xi + \cos 2\widehat{\varphi} - 2),\ y = \sin\widehat{\varphi}(\xi + \cos 2\widehat{\varphi} + 2) \;\middle|\; \widehat{\varphi} \in S^1 \right\}, \quad (13)$$

which is illustrated by Figure 4. The parameter $\widehat{\varphi}$ in (13) coincide with the critical points of potential $W(\varphi)$ at given level ξ, as depicted in Figure 3, in respective points of (x, y) plane:

$$\begin{cases} W(\widehat{\varphi}, x(\widehat{\varphi},\xi), y(\widehat{\varphi},\xi)) = \xi, \\ \frac{\partial}{\partial\varphi} W(\varphi, x(\widehat{\varphi},\xi), y(\widehat{\varphi},\xi))\Big|_{\varphi=\widehat{\varphi}} = 0. \end{cases}$$

The introduced parametric representation is convenient, in particular, for defining the location of cusps and self-intersection points. For cusps $\widehat{\varphi} = \varphi^*$, where φ^* is obtained from the equation $\tan^2\varphi^* = (3+\xi)/(3-\xi)$, which have four roots on S_1. We shall denote these cusps as Y_1,...,Y_4 with the lower index being the number of a quadrant, in which the respective value φ^* lies. Self-intersection points of

$\Gamma(\xi)$ on x axis ($-3 < \xi < -1$) we shall denote as B_1 and B_2 for right and left half-planes respectively. Self-intersection points on y axis ($1 < \xi < 3$) we shall denote as S_1 and S_2 for upper and lower half-planes.

Note: It can be demonstrated, that curves $\Gamma(\xi)$ are the involutes of astroid (10) constructed with tethers of length $3 \pm \xi$ extended from astroid's cusps. This makes $\Gamma(\xi)$ also a family of equidistant curves with the distance $|\xi_a - \xi_b|$ between any two curves $\Gamma(\xi_a)$ and $\Gamma(\xi_b)$.

3.3 Transformation of regions $Q_0(\xi), ..., Q_3(\xi)$ with change of ξ

It should be noted first, that region with a single librating solution $Q_1(\xi)$ is present on plane (x, y) for all values of ξ. Other regions appear and disappear, as ξ crosses several bifurcation values ξ_i:

$$\xi_1 = -3,\ \xi_2 = -1,\ \xi_3 = 1,\ \xi_4 = 3.$$

We shall describe, how the regions are transformed, as ξ increases.

If $\xi < \xi_1$, there exists a forbidden region $Q_0(\xi)$ around the point $(0, 0)$, with the rest of (x, y) plane being the $Q_1(\xi)$ region.

At $\xi = \xi_1$ on the right and on the left from region $Q_0(\xi)$ two parts of region $Q_2(\xi)$ (region with two librating solutions) appear (Fig. 5).

At $\xi = \xi_2$ the region $Q_0(\xi)$ disappears and $Q_2(\xi)$ becomes connected (Fig. 6).

At $\xi = \xi_3$ region $Q_2(\xi)$ is separated into two parts again by appearing region $Q_3(\xi)$ (region with circulating resonant angle) around the point $(0, 0)$ as seen in Figure 7.

At $\xi = \xi_4$ region $Q_2(\xi)$ disappears (Fig. 8). For $\xi > \xi_4$ there exists only region $Q_3(\xi)$ surrounded by $Q_1(\xi)$.

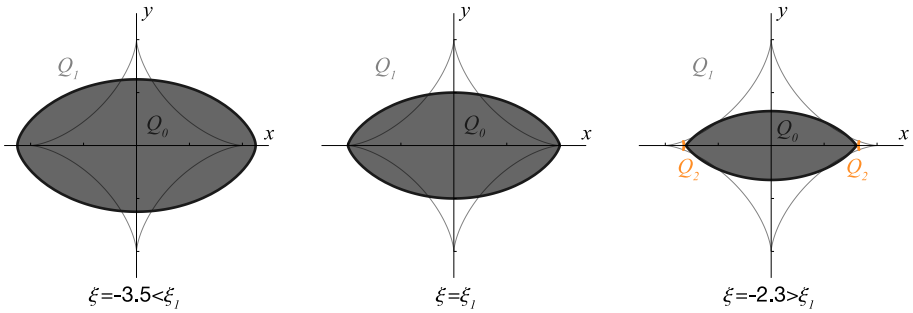


Fig. 5 Bifurcation at $\xi = \xi_1$: appearance of region Q_2. Here and further region Q_0 is colored dark gray, region Q_2 – orange. The rest blank space corresponds to region Q_1

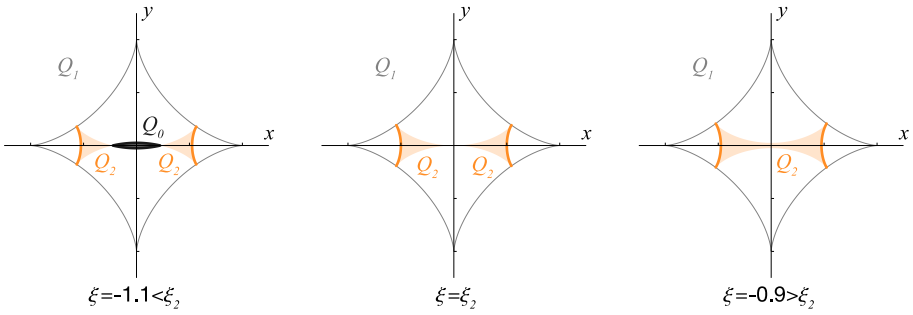


Fig. 6 Bifurcation at $\xi = \xi_2$: vanishing of forbidden region Q_0

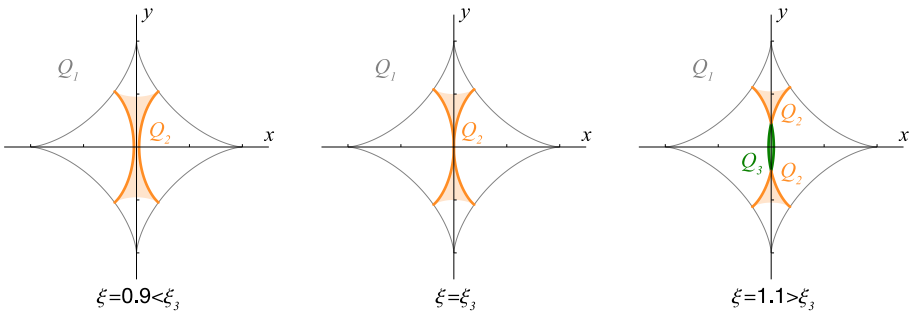


Fig. 7 Bifurcation at $\xi = \xi_3$: appearance of region Q_3 (here and further colored green)

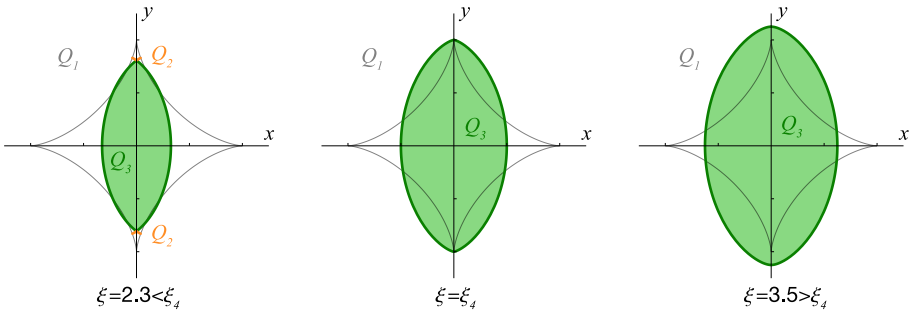


Fig. 8 Bifurcation at $\xi = \xi_4$: vanishing of region Q_2

Let us now describe how borders of regions $Q_0(\xi), ..., Q_3(\xi)$ transforms with increase of ξ. The border between $Q_0(\xi)$ and $Q_1(\xi)$ we shall call the *existence curve* and denote it as $\Gamma_0(\xi)$. It corresponds to the part of the critical curve $\Gamma(\varepsilon)$ in which $W_{min}(x, y) = \xi$. For $\xi < \xi_1$ curve $\Gamma(\varepsilon) \equiv \Gamma_0(\varepsilon)$. For $\xi_1 < \xi < \xi_2$ curve $\Gamma_0(\varepsilon)$ consists of two intervals of $\Gamma(\varepsilon)$, lying between points of self-intersection B_1 and B_2.

We shall adopt the traditional terminology common in studies of slow-fast systems (Wisdom 1985; Neishtadt 1987a) with modifications made to better represent the specifics of the discussed problem. The border between regions $Q_1(\xi)$ and $Q_3(\xi)$ we shall call an *uncertainty curve of the first kind* and use a notation $\Gamma_1(\xi)$ for it. Points of the uncertainty curve of the first kind are defined by condition $W_{\max}(x, y) = \xi$. If $\xi > \xi_4$, then $\Gamma_1(\xi) \equiv \Gamma(\xi)$. For $\xi_3 < \xi < \xi_4$, the curve $\Gamma_1(\xi)$ consists of $\Gamma(\xi)$ parts, which are contained between points of self-intersection S_1 and S_2.

The part of the border between $Q_1(\xi)$ and $Q_3(\xi)$, along which holds the equality $W^*_{\max}(x, y) = \xi$, we shall call an *uncertainty curve of the second kind* and denote it $\Gamma_2(\xi)$. For $\xi_1 < \xi < \xi_3$ the $\Gamma_2(\xi) = Y_1Y_3 \cup Y_2Y_4$, where Y_1Y_3 and Y_2Y_4 are segments of $\Gamma(\xi)$, which lie between corresponding cusps. If $\xi_1 < \xi < \xi_2$ then curve $\Gamma_2(\xi) = S_1Y_1 \cup S_1Y_2 \cup S_2Y_3 \cup S_2Y_4$. For the rest part of the border between $Q_1(\xi)$ and $Q_3(\xi)$ holds $W^*_{\min}(x, y) = \xi$. As no dynamical effects of interest are happening on this segment, we shall not refer to it further.

Figure 9 depicts a diagram, that shows values of $\widehat{\varphi}$ defining positions of cusps and self-intersection points on $\Gamma(\xi)$, as well as the segments which correspond to existence curve and two uncertainty curves. Due to the symmetry, it is sufficient to consider only $\widehat{\varphi} \in [0, \pi/2]$ (Fig. 4).

3.4 Three-dimensional representation of the set of curves $\Gamma(\xi)$

Curves $\Gamma(\xi)$ can be interpreted as cross sections of some surface F in the space $xy\xi$ by equi-Hamiltonian planes $\xi = const$ (Fig. 10a,b). In this space for fixed value of $\widehat{\varphi}$ the equations (13) define a straight line, which means that the surface F is ruled (Fig. 10c).

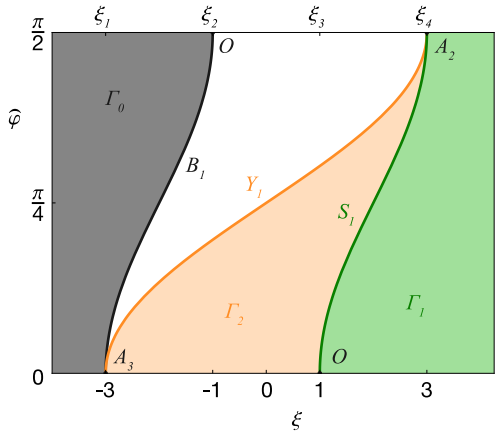


Fig. 9 Diagram showing the partition of critical curve into existence curve $\Gamma_0(\xi)$ and critical curves $\Gamma_{1,2}(\xi)$

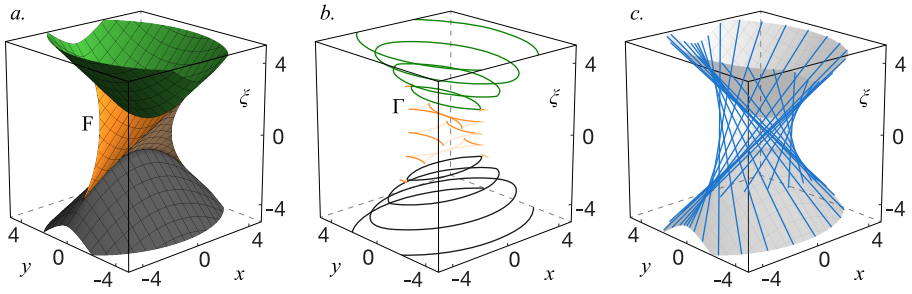


Fig. 10 Surface F composed of curves $\Gamma(\xi)$ in $xy\xi$ space: a. general representation of the surface, b. surface's cross sections by equi-Hamiltonian planes, c. rulings of surface F

The same surface F defined by the equation analogous to (12) also appears in a completely different problem studied by Batkhin (2012), where it partitions the parametric space of some mechanical system into regions with different stability properties.

4 Evolution equations construction

4.1 Averaging along fast subsystem's solutions

Considering that

$$\frac{\partial \Xi}{\partial x} = \cos\varphi, \quad \frac{\partial \Xi}{\partial y} = \sin\varphi,$$

construction of the evolution equations (4) require calculating two averaged properties:

$$\begin{aligned} \langle \sin\varphi \rangle &= \frac{1}{T(x,y,\xi)} \int_0^{T(x,y,\xi)} \sin\varphi(\tau,x,y,\xi)\, d\tau, \\ \langle \cos\varphi \rangle &= \frac{1}{T(x,y,\xi)} \int_0^{T(x,y,\xi)} \cos\varphi(\tau,x,y,\xi)\, d\tau. \end{aligned} \tag{14}$$

The equality

$$\frac{d\varphi}{d\tau} = \Phi = \pm\sqrt{2\left[\xi - W(x,y,\varphi)\right]}$$

allows finding a period of fast subsystem's solution at Hamiltonian level $\Xi = \xi$ and calculating (after proper change of variables) values of integrals on the right-hand side of (14), e.g. for librating solutions:

$$\begin{array}{c} T(x,y,\xi) = 2\int\limits_{\varphi_*}^{\varphi^*} \frac{d\varphi}{\sqrt{2[\xi - W(x,y,\varphi)]}}, \\ \int\limits_0^{T(x,y,\xi)} f\left(\varphi(t,x,y,\xi)\right) d\tau = 2\int\limits_{\varphi_*}^{\varphi^*} \frac{f(\varphi) d\varphi}{\sqrt{2[\xi - W(x,y,\varphi)]}}. \end{array} \tag{15}$$

Here φ_* and φ^* denote minimum and maximum values of angle φ in librating solution, along which the averaging is being performed.

For the system (2) period $T(x,y,\xi)$ and integrals (14) can be expressed in terms of complete elliptical integrals of the first and the third kind. Further the concise description of this transformation is given, using the case

$$-\pi \le \varphi_* < \varphi^* \le \pi \tag{16}$$

as an example. After standard substitution $\lambda = \tan(\varphi/2)$ we obtain

$$\begin{array}{rl} T(x,y,\xi) = & 4\int\limits_{\lambda_*}^{\lambda^*} \frac{d\lambda}{\sqrt{2R_4(\lambda)}}, \\ \langle \sin\varphi \rangle = \int\limits_{\varphi_*}^{\varphi^*} \frac{\sin\varphi d\varphi}{\sqrt{2[\xi - W(x,y,\varphi)]}} = & 4\int\limits_{\lambda_*}^{\lambda^*} \frac{\lambda d\lambda}{(1+\lambda^2)\sqrt{2R_4(\lambda)}}, \\ \langle \cos\varphi \rangle = \int\limits_{\varphi_*}^{\varphi^*} \frac{\cos\varphi d\varphi}{\sqrt{2[\xi - W(x,y,\varphi)]}} = & 2\int\limits_{\lambda_*}^{\lambda^*} \frac{\left(1-\lambda^2\right) d\lambda}{(1+\lambda^2)\sqrt{2R_4(\lambda)}}. \end{array} \tag{17}$$

Here $\lambda_* = \tan(\varphi_*/2)$, $\lambda^* = \tan(\varphi^*/2)$. Function $R_4(\lambda)$ in (17) is a quartic polynomial

$$R_4(\lambda) = d_0\lambda^4 + d_1\lambda^3 + d_2\lambda^2 + d_3\lambda + d_4$$

with coefficients

$$d_0 = \xi - 1 + x, \quad d_1 = d_3 = -2y, \quad d_2 = 2\xi + 6, \quad d_4 = \xi - 1 - x.$$

Integrals on the right-hand side in (17) can be rewritten as follows:

$$\begin{array}{l} T(x,y,\xi) = \frac{4}{\sqrt{2|d_0|}} I_{0,0}, \\ \int\limits_{\varphi_*}^{\varphi^*} \frac{\sin\varphi d\varphi}{\sqrt{2[\xi - W(x,y,\varphi)]}} = \frac{4}{\sqrt{2|d_0|}} I_{1,1}, \\ \int\limits_{\varphi_*}^{\varphi^*} \frac{\cos\varphi d\varphi}{\sqrt{2[\xi - W(x,y,\varphi)]}} = \frac{2}{\sqrt{2|d_0|}} \left(2I_{1,0} - I_{0,0}\right), \end{array} \tag{18}$$

where notation $I_{k,r}$ is used for integrals:

$$I_{k,r} = \int\limits_{\lambda_*}^{\lambda^*} \frac{\lambda^r d\lambda}{(\lambda^2+1)^k \sqrt{\pm(\lambda - a_1)(\lambda - a_2)(\lambda - a_3)(\lambda - a_4)}}. \tag{19}$$

a_k – roots of polinomial $R_4(\lambda)$, and the sign in the square root is determined by sign of coefficient d_0. Integrals (19) can be presented as linear combinations of elliptic integrals of the first and the third kind:

$$\begin{array}{l} I_{0,0} = c_{0,0} K(k), \\ I_{1,0} = c_{1,1} K(k) + c_{1,3} \Pi\left(h,k\right) + \bar{c}_{1,3} \Pi\left(\bar{h},k\right), \\ I_{1,1} = g_{1,1} K(k) + g_{1,3} \Pi\left(h,k\right) + \bar{g}_{1,3} \Pi\left(\bar{h},k\right). \end{array} \tag{20}$$

Analytical expressions for coefficients $c_{m,l}$, $g_{m,l}$, moduli k, and parameters h in (20) depend on integration interval and properties of $R_4(\lambda)$ roots. These expressions are gathered in the Appendix B.

Expressions of the kind

$$c\Pi(h,k)+\bar{c}\Pi(\bar{h},k)\quad (c,h\in\mathbb{C},\ k\in\mathbb{R},\ 0<k^2<1)$$

can be further reduced to linear combinations of complete elliptic integrals of the first kind and the third kind with real parameter (Byrd and Friedman 1954; Lang and Stevens 1960). This, however, results in more complicated expressions, which is why we use representation (20).

When averaging along librating solutions of fast subsystem, which violate the condition (16), after substitution $\lambda=\tan(\varphi/2)$ the integration in (17) is carried over two semi-infinite intervals. E.g., for $\varphi_*<\pi,\ \varphi^*>\pi,\ \varphi^*-\varphi_*<2\pi$ the expression for the period T is

$$T(x,y,\xi)=4\left(\int\limits_{-\infty}^{\lambda^*}\frac{d\lambda}{\sqrt{2R_4(\lambda)}}+\int\limits_{\lambda_*}^{+\infty}\frac{d\lambda}{\sqrt{2R_4(\lambda)}}\right).$$

In these cases it is implied that all $I_{k,r}$ in (18) are the sum of two integrals as well.

After all described transformations evolution equations (4) take a simple form

$$\frac{dx}{d\tau}=\varepsilon\frac{2I_{1,1}}{I_{0,0}},\quad \frac{dy}{d\tau}=\varepsilon\left[1-\frac{2I_{1,0}}{I_{0,0}}\right]. \tag{21}$$

It should be noted, that there is an ambiguity in calculation of the right-hand side parts of evolution equations in the region $Q_2(\xi)$: the result depends on the choice of the fast subsystem's solution, and there are two different librating solutions in $Q_2(\xi)$. Consequently, phase portraits of (4) shall contain two sets of trajectories in $Q_2(\xi)$, which correspond to two possible variants of slow variables' evolution.

When describing the crossing of uncertainty curves $\Gamma_i(\xi)$ by the projection $\boldsymbol{\zeta}(\tau)=(x(\tau),y(\tau))^T$ of the phase point $\mathbf{z}(\tau)=(\varphi(\tau),\Phi(\tau),x(\tau),y(\tau))^T$ on the plane (x,y), we shall confine ourselves to formal continuation of averaged system's trajectories, lying on opposite sides of Γ_i. The detailed analysis of these events is given in Neishtadt (1987a), Neishtadt and Sidorenko (2004), and Sidorenko et al. (2014).

4.2 Fast subsystem's action variable – integral of evolution equations

As was mentioned in the Section 2, adiabatic invariant $J(x,y,\xi)$ of slow-fast system is a first integral of evolution equations (4). Formula (6) for $J(x,y,\xi)$ can be expressed as a linear combination of integrals $I_{k,r}$ defined by (19):

$$J(x,y,\xi)=\frac{1}{\pi}\int\limits_{\varphi_*}^{\varphi^*}\Phi d\varphi=\frac{1}{\pi}\int\limits_{\varphi_*}^{\varphi^*}\sqrt{2\left[\xi-W(x,y,\varphi)\right]}d\varphi=\frac{2}{\pi}\int\limits_{\lambda_*}^{\lambda^*}\frac{\sqrt{2R_4(\lambda)}d\lambda}{(1+\lambda^2)^2}=$$

$$=\frac{2\sqrt{2}}{\pi\sqrt{|d_0|}}\left[d_0I_{0,0}+d_1I_{1,1}+(d_2-2d_0)I_{1,0}+(d_4+d_0-d_2)I_{2,0}\right]. \tag{22}$$

Analytical expression for $I_{2,0}$ is presented in the Appendix B alongside the rest of the integrals previously shown in (20).

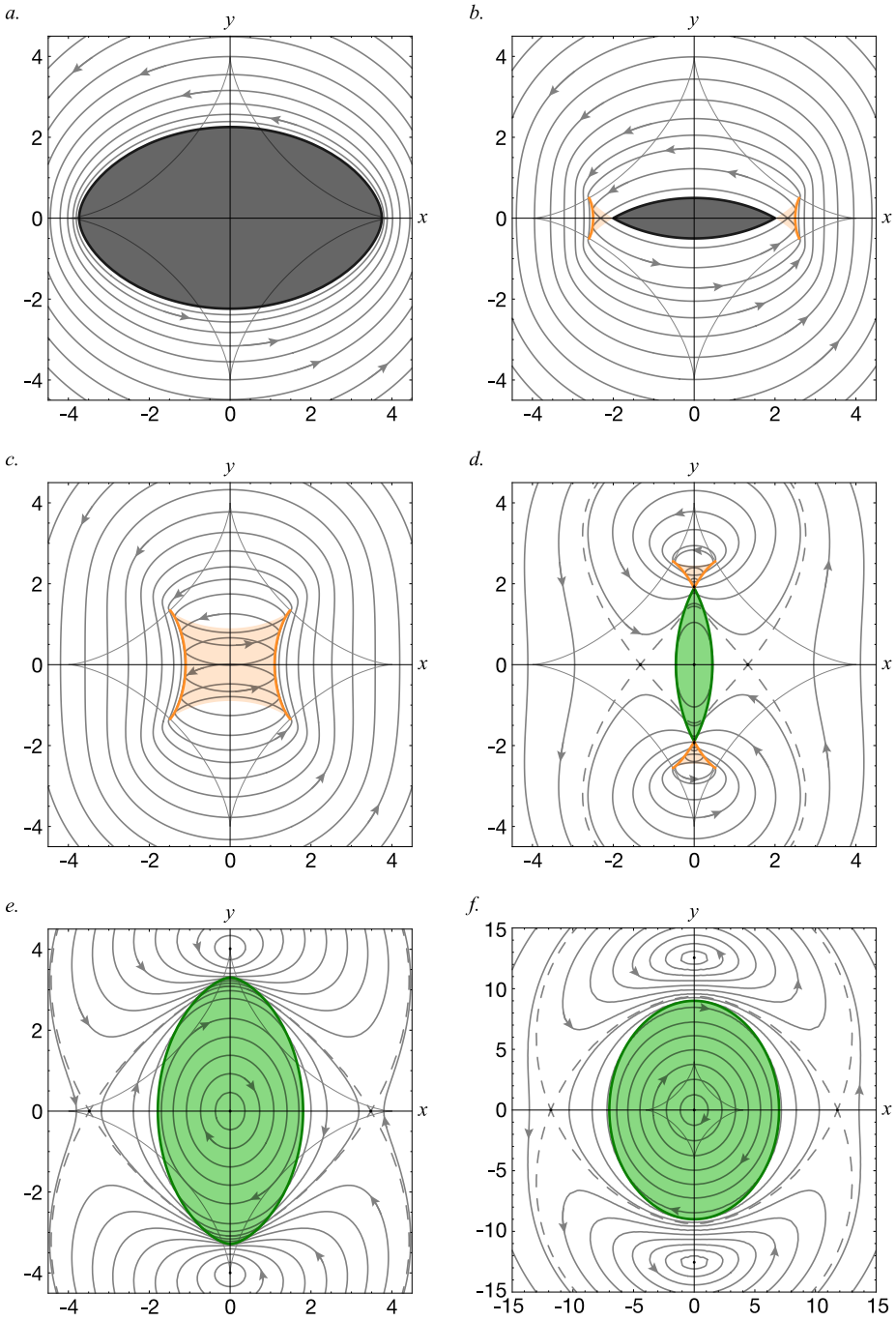


Fig. 11 Phase portraits of evolution equations:
a. $\xi = -4$, b. $\xi = -1.5$, c. $\xi = -0.1$, d. $\xi = 1.45$, e. $\xi = 3.4$, f. $\xi = 8.0$

5 Study of slow variables' behavior using evolution equations

5.1 Phase portraits of evolution equations. Stationary points

To analyze solutions of the slow subsystem (4), we build its phase portraits. For values $\xi < \xi_1$ the structure of phase portrait is simple – all phase trajectories are represented by closed loops encircling the forbidden region $Q_0(\xi)$ (Fig. 11a). Figure 11b depicts a typical phase portrait for $\xi \in (\xi_1, \xi_2)$ – two symmetrical parts of region $Q_2(\xi)$ adjoining the central region $Q_0(\xi)$ contain two layers of phase trajectories. For $\xi \in (\xi_2, \xi_3)$ there are only two regions on the phase plane, i.e. $Q_0(\xi)$ and $Q_2(\xi)$ (Fig. 11c). In addition to presented in Figure 11c,d change of phase portrait's global structure, the behaviour of phase trajectories near the uncertainty curves $\Gamma_{1,2}(\xi)$ at $\xi \in (\xi_2, \xi_4)$ have some specific qualitative differences at different ξ values. The detailed description of that is given in the end of this section.

Phase portraits at $\xi > \xi_3$ have five stationary points: the origin of xy-plane is the stable point of the center type, two more center points are symmetrically located on the y-axis, and two unstable saddle points are symmetrically located on the x-axis (Fig. 11d–f). Phase portraits depicted in Figures 11e and 11f are differ in relative positions of heteroclinic trajectories and uncertainty curve Γ_1.

Ordinates y of the center points above and below plane's origin are defined by equation

$$K\,(m) = 2\Pi\,(n\,|m\,)\,, \tag{23}$$

where

$$m = \frac{U_+}{U_-}, \quad n = \frac{U_+}{\xi + 1 - |y|}, \quad U_\pm = \xi - 3 \pm \sqrt{y^2 + 8(1-\xi)}.$$

Abscissae x of the saddle points are defined by the same relation (23) with different parameters:

$$m = \frac{Q_{+-}}{Q_{--}}\frac{Q_{++}}{Q_{-+}}, \quad n = \frac{Q_{+-}}{Q_{--}}, \quad Q_{\pm\pm} = \sqrt{x^2 + 8(1+\xi)} \pm 4 \pm |x|.$$

Solutions of (23) are plotted in Figure 12 as functions of ξ for both types of stationary points. Note, that top and bottom center points are located in Q_2 at $\xi < \xi_5 = 2$ and in Q_1 at $\xi > \xi_5$ (Fig. 13).

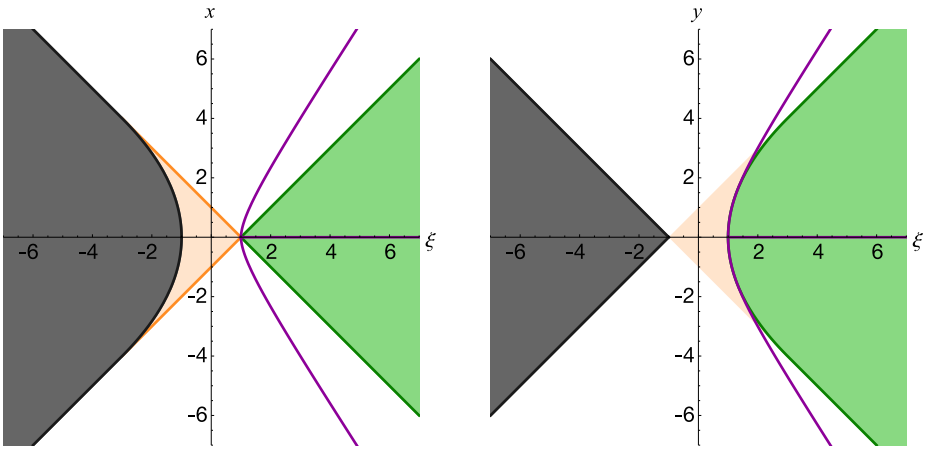


Fig. 12 Coordinates of evolution equations' stationary points, which lie on axis x (left), and on axis y (right). Values of coordinates as functions of ξ are represented by violet lines. The rest of the coloring is consistent with Figure 11 in denoting the regions Q_i and points from different parts of the critical curve

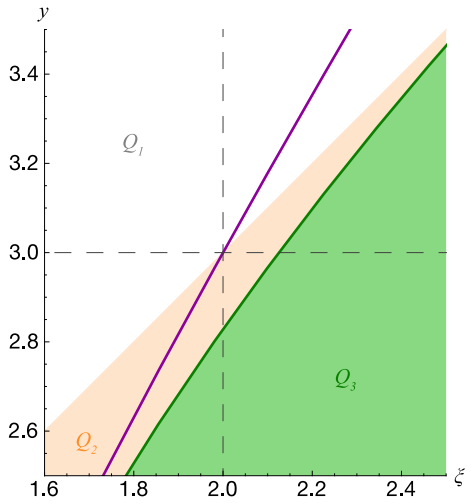


Fig. 13 Transition of the top center point from $Q_2(\xi)$ to $Q_1(\xi)$ at $\xi = \xi_5 = 2$

5.2 Limiting points on uncertainty curves

To conclude the description of how phase portraits' topology changes with ξ value, points of uncertainty curves' intersections with limiting trajectories, that are limiting cases for different families of trajectories, should be considered. We shall refer to them as *limiting points*.

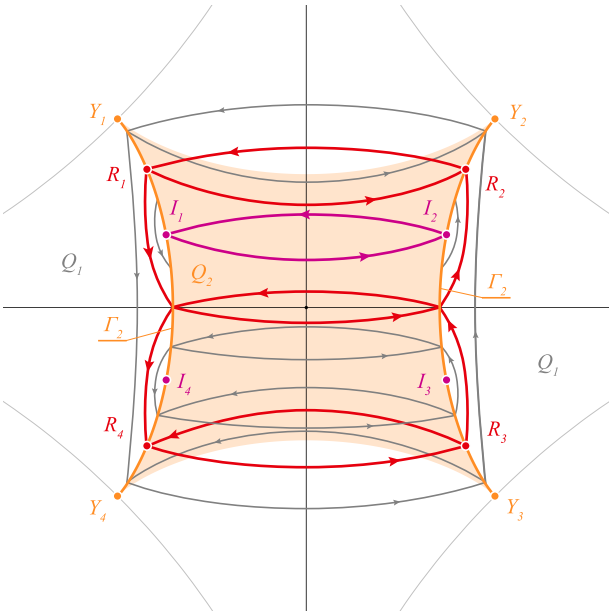


Fig. 14 Limiting points R_i and I_i at $\xi \approx 0$

Several types of limiting points are depicted in Figure 14. Trajectories, which go in Q_1 between two points on uncertainty curve Γ_2, can be divided into two families: the trajectories that intersect x axis, and those that do not. Thus there is limiting trajectory that separates these two families (in Figure 14 it is colored red). We shall denote the limiting points corresponding to this trajectory as $R_1, ..., R_4$ (Fig. 14).

The subset of trajectories, which do not cross x-axis in Q_1 as another limiting case contain trajectories, which come to uncertainty curve from the side of Q_2 and then reflect back without exiting to Q_1. In Figure 14 these trajectories are colored purple, and the corresponding limiting points are denoted $I_1, ..., I_4$.

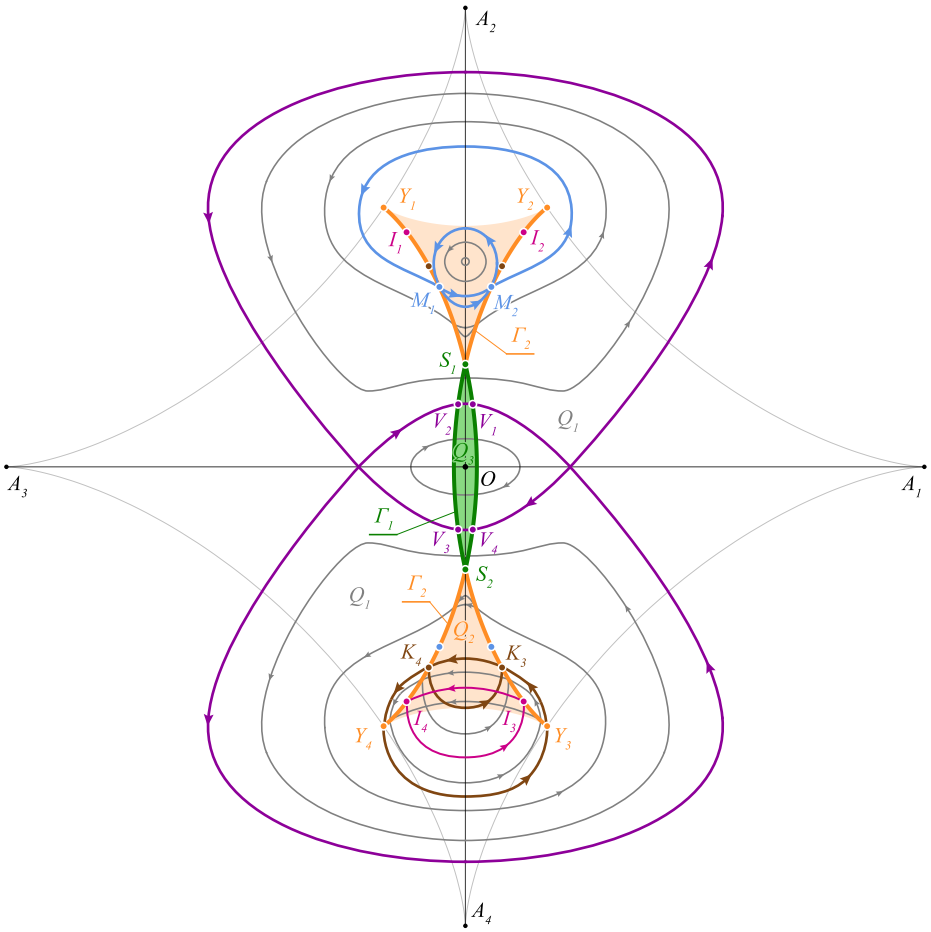


Fig. 15 Limiting points K_i, M_i and V_i ($\xi \sim 1.5$)

More limiting points are depicted in figure 15. Points $K_1, ..., K_4 \in \Gamma_2$ are connected to cusps $Y_1, ..., Y_4$ by limiting phase trajectories, which separate the family of trajectories lying to the one side of uncertainty curve Γ_2 from those which in Q_1 connect symmetric points on left and right sides of uncertainty curves $\Gamma_{1,2}$. Limiting points $M_1, ..., M_4$ divides each of four Γ_2 segments (located in each of four quadrants of xy plane) into two sections: one section has both trajectories, which adjoin from Q_2 side, going in the same direction, while trajectories adjoining the other section go in opposite directions (also see Figure 19). Points $V_1, ..., V_4$ of Γ_1 curve's intersections with mentioned earlier separatrices constitute the last type of limiting points.

All differences between the phase portraits (Fig. 11) emerge from changes in position of limiting points on the critical curve. By adding these points to diagram in Figure 9 we obtain a bifurcation diagram (Fig. 16), from which all changes in topological structure of phase portraits can be understood. Let us describe, what is happening to different limiting points by going successively from low to high values of ξ. The first limiting points – R_i and I_i – appear at $\xi = \xi_6 \approx -0.22073$. At $\xi = \xi_7 \approx 0.27704$ points R_i merge with cusps Y_i, and at the same time points K_i appear. Points M_i and V_i emerge simultaneously with region Q_3 and self-intersections points S_i of the critical curve at $\xi = \xi_3$. All points on the Γ_2 part of

the critical curve – I_i, K_i, and M_i, as well as the ends Y_i, S_i of Γ_2 itself – disappear at $\xi = \xi_4$ merging with the astroid's cusps A_2 and A_4. Finally, at $\xi = \xi_8 \approx 5.57954$ points V_i disappear by merging pairwise.

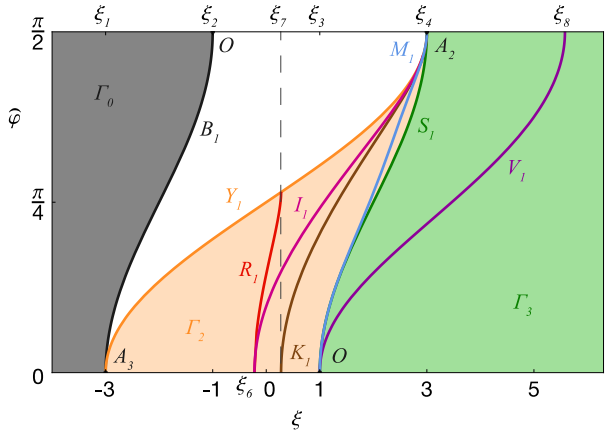


Fig. 16 Bifurcation diagram showing the dependance of limiting points position on the critical curve Γ on ξ.

Bifurcation Hamiltonian values $\xi_1, \ldots, \xi_8$ partition the whole range of ξ into nine intervals, meaning that there is a total number of nine different types of phase portraits for slow subsystem. The bifurcation at ξ_5 (Fig. 13) is omitted from Figure 16 because it does not bear any significance for the dynamical effects considered further.

6 Quasi-random effects

6.1 Probabilistic change of fast subsystem's motion regime on the uncertainty curve of the second kind

In each point of $\Gamma_2(\xi)$ three *guiding trajectories*, i.e. trajectories of averaged system (4), meet: two on the side of $Q_2(\xi)$ region and one on the $Q_1(\xi)$ side. In the case, when two out of these three trajectories are outgoing, the transition of the phase point to either one of them can be considered as a probabilistic event. In the original system (1) initial values of fast variables corresponding to two different outcomes are strongly mixed in the phase space. Therefore even small variation of initial conditions $\mathbf{z}(0) = (\varphi(0), \Phi(0), x(0), y(0))^T$ can lead to qualitative change in system's evolution. As an example, Figure 17 depicts projections on the plane (x, y) of two trajectories $\gamma_{1,2}$, obtained as solutions of the system (1) with close initial conditions. Both trajectories approach uncertainty curve along the same guiding trajectory, but diverge after that – γ_1 exits $Q_2(\xi)$ and follows the outgoing guiding trajectory in $Q_1(\xi)$, while γ_2 turns and goes back along the other guiding trajectory in $Q_2(\xi)$.

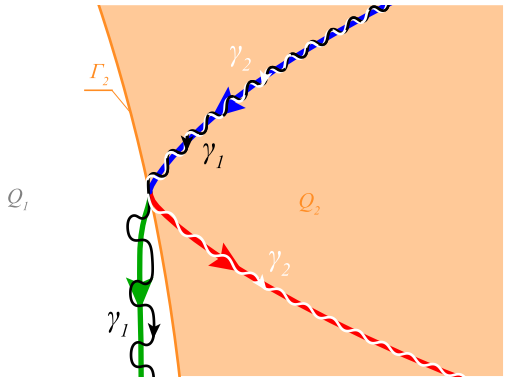


Fig. 17 Two phase trajectories starting from very close initial conditions may diverge at uncertainty curve Γ_2, as γ_1 and γ_2 do. Green and red lines show two guiding trajectories departing from the same point of Γ_2, to which the blue one arrives. Trajectory γ of non-averaged system may go along either one of them after reaching the border between Q_1 and Q_2

In deterministic systems with strongly entangled trajectories the probability of a specific outcome is determined by the fraction of phase volume occupied by corresponding initial conditions (formal definition can be found in Arnold (1963) and Neishtadt (1987b)). In order to find the probabilities of transitions to different outgoing trajectories in some point (x_*, y_*) on Γ_2, two auxiliary parameters must be calculated first (Neishtadt 1987b; Artemyev et al. 2013):

$$\Theta_{1,2} = \int\limits_{-\infty}^{+\infty} \left(\frac{\partial W^*_{\max}}{\partial x}\frac{\partial W}{\partial y} - \frac{\partial W^*_{\max}}{\partial y}\frac{\partial W}{\partial x} \right)_{\varphi^s_{1,2}(t,x_*,y_*,\xi)} d\tau. \tag{24}$$

These parameters have a meaning of rates with which areas bounded by separatrices $(\varphi^s_1(\tau, x_*, y_*, \xi), \Phi^s_1(\tau, x_*, y_*, \xi))$ and $(\varphi^s_2(\tau, x_*, y_*, \xi), \Phi^s_2(\tau, x_*, y_*, \xi))$ in fast variables' phase space change. After substitution of specific potential function (2) into (24) and change of integration variable to φ we obtain:

$$\Theta_1 = 2\int\limits_{\varphi^s_{\min}}^{\widehat{\varphi}} \frac{\sin(\varphi - \widehat{\varphi})}{\sqrt{2\left(\xi - W(x_*, y_*, \varphi)\right)}} d\varphi, \quad \Theta_2 = 2\int\limits_{\widehat{\varphi}}^{\varphi^s_{\max}} \frac{\sin(\varphi - \widehat{\varphi})}{\sqrt{2\left(\xi - W(x_*, y_*, \varphi)\right)}} d\varphi. \tag{25}$$

Here $\widehat{\varphi}$ is the coordinate φ of the saddle point in the fast subsystem's phase portrait (it coincides with the value $\widehat{\varphi}$ corresponding to point (x_*, y_*) in (13)); $\varphi^s_{\min}$ and $\varphi^s_{\max}$ are the minimal and the maximal values of φ in homoclinic trajectories to the left and to the right of the saddle point respectively. Applying the substitution $\lambda = \cot[(\varphi - \widehat{\varphi})/2]$ to (25) we obtain:

$$\Theta_{1,2} = \frac{4}{\sqrt{A}} \int\limits_{\lambda_{\min}}^{\lambda_{\max}} \frac{\lambda\, d\lambda}{(1+\lambda^2)\sqrt{(\lambda - a)(\lambda - b)}}, \tag{26}$$

where

$$a = \frac{B - \sqrt{B^2 - AC}}{A}, \quad b = \frac{B + \sqrt{B^2 - AC}}{A},$$

$$A = \xi + 3\cos(2\widehat{\varphi}), \quad B = 2\sin(2\widehat{\varphi}), \quad C = \xi - \cos(2\widehat{\varphi}).$$

It should be noted, that inequalities $A > 0$ and $B^2 > AC$ hold for all points of Γ_2. Integration in (26) is carried out over the intervals $(-\infty, a)$ and $(b, +\infty)$ for Θ_1 and Θ_1 respectively. The result can be obtained by using Cauchy's residue theorem:

$$\Theta_1 = \frac{4}{\sqrt{A}}\mathrm{Re}\left(\frac{L - i\pi}{\alpha\beta}\right), \quad \Theta_2 = \frac{4}{\sqrt{A}}\mathrm{Re}\left(\frac{L}{\alpha\beta}\right).$$

Here

$$L = \ln\left(\frac{b-a}{(\alpha-\beta)^2}\right), \quad \alpha = \sqrt{a+i}, \quad \beta = \sqrt{b+i},$$

and the branches of multifunctions are selected in such way, that $\mathrm{Im}(L)$, $\arg(\alpha)$, and $\arg(\beta) \in (0, \pi)$.

Now we can write down the expressions for probabilities of different evolution scenarios for a phase point on $\Gamma_2(\xi)$. Let us denote the probability of point going to region $Q_1(\xi)$ as P_0, and probabilities corresponding to two trajectories going inside $Q_2(\xi)$ as P_1 and P_2. The resulting formulae (Artemyev et al. 2013) take a form:

$$P_0 = 1 - P_1 - P_2, \quad P_1 = \max(\Theta_1, 0)/\Theta_\Sigma, \quad P_2 = \max(\Theta_2, 0)/\Theta_\Sigma, \tag{27}$$

where

$$\Theta_\Sigma = \max(\Theta_1, 0) + \max(\Theta_2, 0) + \max(-\Theta_1 - \Theta_2, 0).$$

In Figure 18 and Figure 19 change of probabilities (27) along Γ_2 is shown alongside with phase portraits at corresponding values of Hamiltonian and limiting points, which mark the change of sign in $\Theta_{1,2}$ or $\Theta_1 + \Theta_2$.

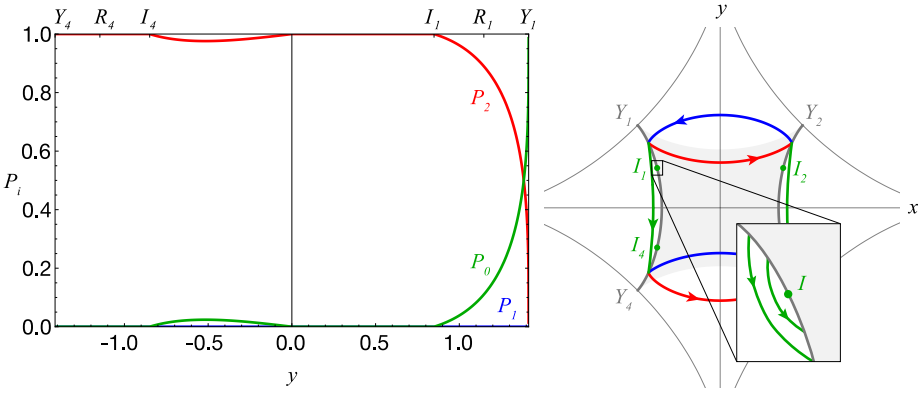


Fig. 18 Change of P_i along Y_4Y_1 segment of Γ_2 at $\xi = 0$. The graph for Y_2Y_3 can be reconstructed by the symmetry, changing the y sign and swapping red and blue plots. In $I_1, \ldots, I_4$ the sum $\Theta_1 + \Theta_2 = 0$, which results in P_1 plot sticking to 0 on one side from these points

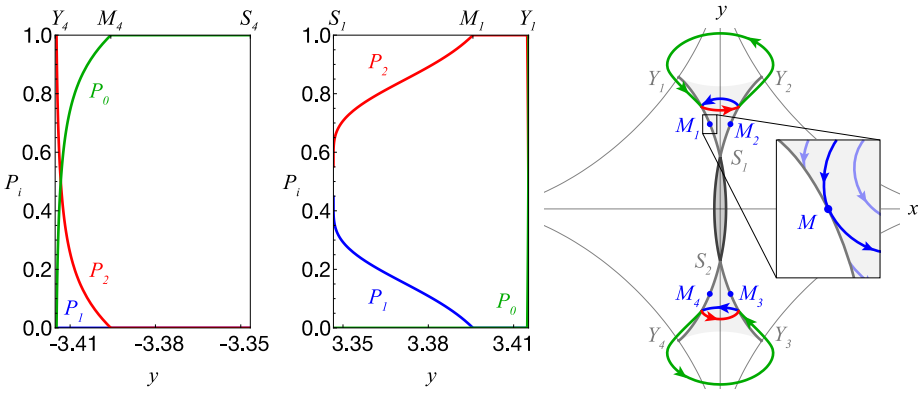


Fig. 19 Change of P_i along segments Y_4S_2 and S_1Y_1 of Γ_2 at $\xi = 2.4$. In $M_{1,2}$ parameter $\Theta_1 = 0$, and in $M_{3,4}$ parameter $\Theta_2 = 0$, which results in singularities of probabilities plots in these limiting points

6.2 Adiabatic chaos

Adiabatic chaos emerges due to non-applicability of adiabatic approximation near the uncertainty curve. As a result the projection of phase point $\boldsymbol{\zeta}(\tau) = (x(\tau), y(\tau))^T$ leaves the vicinity of uncertainty curve along the guiding trajectory, which slightly differs from the direct continuation of approach trajectory (Fig. 20). The resulting offset between incoming and outgoing guiding trajectories can be treated as a quasi-random jump with order of magnitude $\varepsilon\,|\ln\varepsilon|$ (Tennyson et al. 1986; Neishtadt 1987b,a).

As a result of persistent jumps any trajectory that crosses the uncertainty curve after a long time will fill a whole region of phase plane, which we will call an *adiabatic chaos region* (Fig. 21). This region consists of points belonging to trajectories, which cross the uncertainty curve.

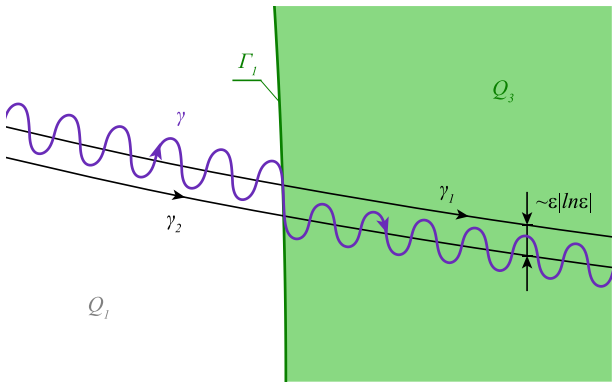


Fig. 20 The jump of trajectory γ from guiding trajectory γ_1 to γ_2 upon crossing the uncertainty curve

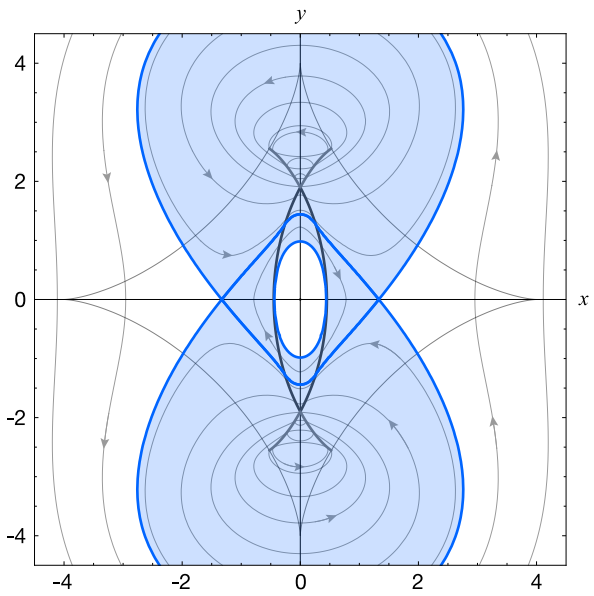


Fig. 21 Adiabatic chaos region at $\xi = 1.45$

At $\xi \in (\xi_3, \xi_8)$ the uncertainty curve is crossed by the separatrices, which connect two saddle points. A phase point projection moving along a guiding trajectory close to separatrix, when crossing the uncertainty

curve, may jump over the separatrix and begin to move along the other guiding trajectory belonging to completely different family. Thus the properties of long-term evolution are suddenly changed on a qualitative level. E.g., in Figure 21 the motion of a phase point projection $\boldsymbol{\zeta}(\tau)$ circling around the coordinate origin in the central part of adiabatic chaos region by crossing the separatrix may transform into circulation in opposite direction around one of two center points (23), which lie on y-axis in upper or lower half-plane. This event can be interpreted as a capture into Kozai-Lidov resonance and it is accompanied by decrease of average inclination value, about which the long-term oscillations occur.

7 Numerical simulations

Construction of the discussed analytical model involved several assumptions that may seem loose. It is thus required to test whether the model can be applied to orbital dynamics of real life objects and these assumptions were not overly restrictive.

For this purpose we used Mercury integrator (Chambers 1999) and carried out several numerical simulations of the Solar system composed of the Sun, the four giant planets, and about 700 known Kuiper belt objects (KBO) near $1:2$, $2:3$, and $3:4$ resonances with Neptune represented by test particles (masses of four inner planets were added to the Sun in order to facilitate the integration). Total time of integration 15 Myr is one order of magnitude larger then the characteristic time $T_N/\varepsilon^2 \approx 1.6$ Myr of slow variables evolution (given the orbital period of Neptune $T_N \approx 160$ y and Neptune/Sun mass ratio defining the small parameter $\varepsilon^2 \sim 10^{-4}$).

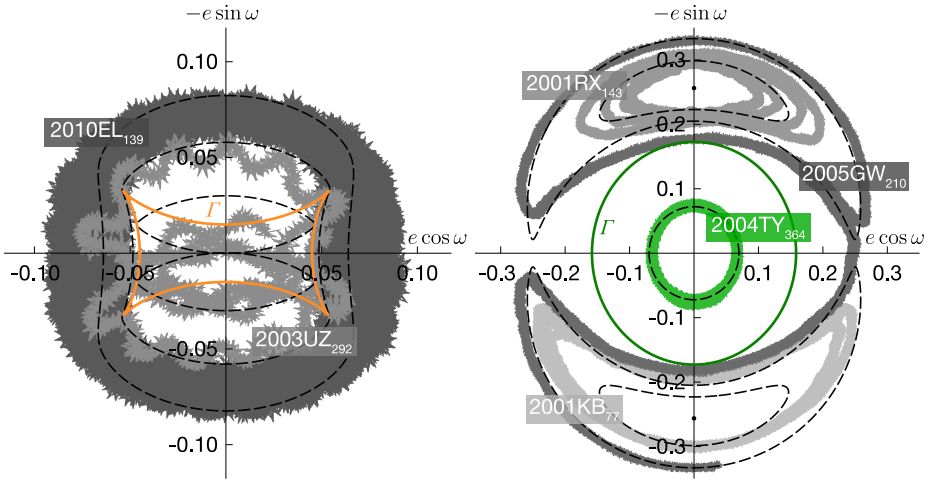


Fig. 22 Comparison of the Solar system's numerical integration with analytical model. Several Kuiper belt objects with Hamiltonian values close to $\xi \approx -0.5$ (left) and $\xi \approx 23$ (right) are plotted on the plane of slow variables. Phase trajectories of the model plotted by dashed lines

For interpretation of the simulation results we shall utilize a scaled version of previously used slow variables:

$$x \propto e\cos\omega, \quad y \propto -e\sin\omega.$$

For exact relations between (e,ω) and (x,y), as well as the expression for small parameter ε, see Appendix A.

Phase trajectories of several objects are plotted in Figure 22. Main sources of difference between analytical phase portraits and numerical ones are non-zero eccentricity of Neptune ($e' \approx 0.01$), high eccentricity of KBOs (up to 0.3 on the right side of Figure 22), and presence of other planets, which introduce additional disturbances distorting the phase plane. Nevertheless, it is clear that the overall

topological structure of phase portraits is reproduced in analytical model. Note, that in restricted three-body problem all solutions of Sessin and Ferraz-Mello (1984) on the same phase plane would be represented by concentric circles with $e = const$ and ω changing linearly with time.

The principal difference between our model and the one introduced by Sessin and Ferraz-Mello (1984) is the expansion of disturbing function past the first term in the Fourier series. Thus we can assert, that the region of the complete phase space, where the second term influences the dynamics in a substantial way, is significantly large. Indeed about 10% of objects in our simulations deviated from circular trajectories in projection on the plane of slow variables. The rest correspond to very high or very low values of ξ, at which all trajectories in Q_1 and Q_3, as well as the curve Γ separating them, in our model are likewise very close to circles.

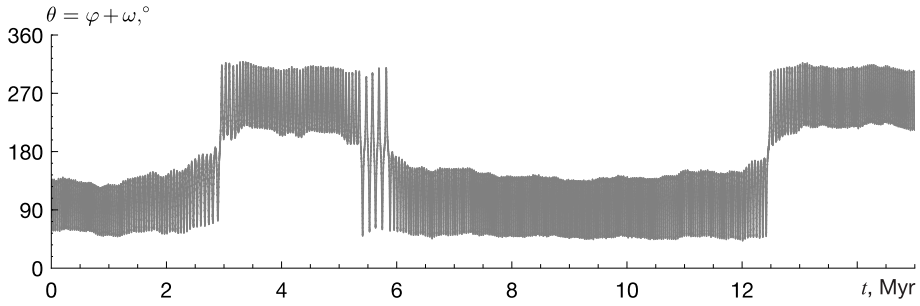


Fig. 23 Resonant angle of $2011UG_{411}$ vs time, demonstrating jumps between two different librating solutions in Q_2

Some effects, that can be derived from the analytical model, are also observed in numerical simulations within the pool of selected KBOs. E.g. resonant angle of $2011UG_{411}$ shows jumps between two different librating regimes characteristic to motion in region Q_2 (Fig. 23), while $2007JJ_{43}$ demonstrates the intermittent behaviour (Fig. 24) with the resonance angle constantly switching between libration and circulation. Phase trajectory of $2007JJ_{43}$ on the plane of slow variables is presented in Figure 25, showing that changes in resonant angle behaviour are conditioned by secular trajectory crossing of the critical curve Γ. Similarly, analytical trajectory γ_0 goes between regions of libration and circulation of resonant angle (Fig. 25). To compensate for angle ω precession on this kind of trajectories the modified resonant angle $\theta = \varphi + \omega$ was used in previous plots[1]. Same as φ, resonant angle θ circulates in Q_3 and librates in Q_1 and Q_2.

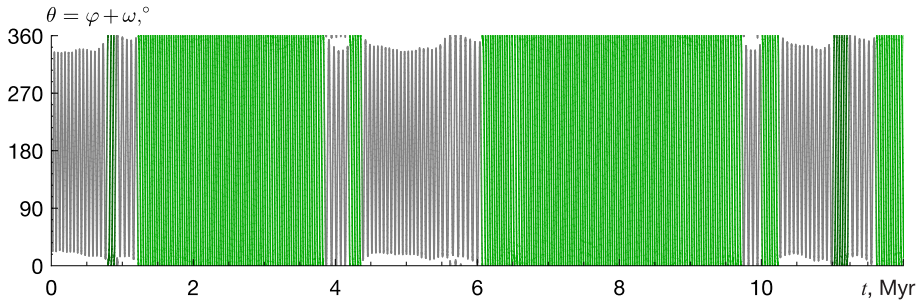


Fig. 24 Resonant angle of $2007JJ_{43}$ vs time. Intervals of circulation and libration colored green and gray respectively

[1] The resonant angle θ is the "standard" one for studies of first-order MMR (Murray and Dermott 2000). Our choice of the resonant angle φ was determined by the desire to write down the Hamiltonian of the system in the form (2), which seem to us most convenient for the analysis.

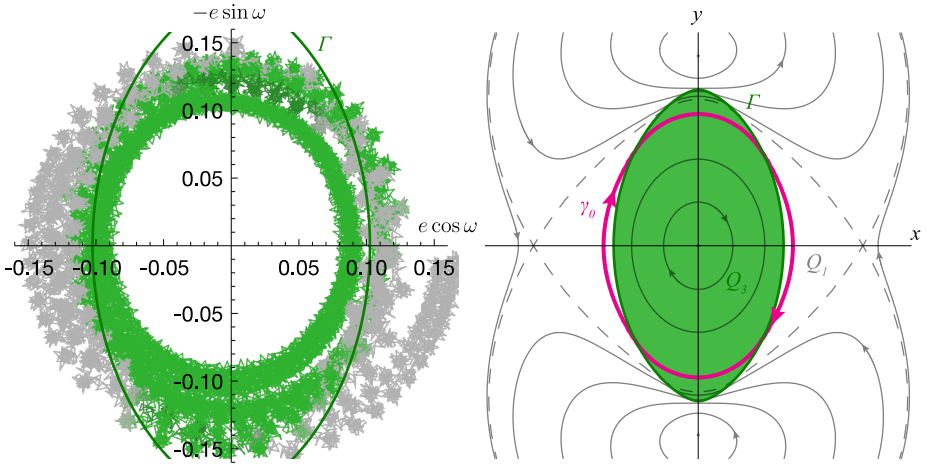


Fig. 25 Phase trajectory of $2007JJ_{43}$ alongside the analogous trajectory γ_0 on the analytical phase portrait. Intervals of resonant angle circulation and libration on the left panel are colored green and gray respectively. It is seen, that the green segments of the trajectory concentrate inside the region bound by Γ, while the gray ones mostly lie outside of it

8 Conclusion

In this paper, using the averaging technique, we study Hamiltonian system that approximately describes the dynamics of a three-body system in first-order MMR (within the restricted circular problem). Our model incorporates harmonics of the Fourier series expansion of disturbing function up to the second order. Thus it can accurately describe the dynamics in that part of the phase space where first two harmonics have comparable magnitudes, and where the well known integrable model of first-order MMR is not applicable. This is the region, from which chaos emerges.

The nonintegrability of our model does not become an obstacle for a detailed analytical investigation of its properties. In particular, we have constructed bifurcation diagrams and phase portraits characterizing the long-term dynamics on different level sets defined by the system's Hamiltonian and obtained expressions for probabilities of quasi-random transitions between different phase trajectories.

The important question is the scope of the correctness of proposed model. We will try to answer it in subsequent studies, using Wisdom's approach to investigate several first-order MMRs without truncating the averaged disturbing function. Nevertheless, even now we can note that the secular evolution of some Kuiper belt objects qualitatively resembles what our simple model predicts.

We hope also that our investigation outlines an approach which can be applied for analysis of similar degeneracy of the averaged disturbing function in the case of other MMRs (e.g., Sidorenko (2006)).

Appendix A: Constructing a model system, that reveals the origin of chaos in first-order MMR

We shall confine ourselves to a case of exterior resonance $p : (p + 1)$ in restricted three-body problem. The interior resonance $(p+1) : p$ can be reduced to the same model using similar approach. The distance between the two major bodies, i.e. a star and a planet, and the sum of their masses are taken here as units of length and mass. The unit of time is chosen such that the orbital period of major bodies' rotation about barycenter is equal to 2π. The mass of the planet μ is considered to be a small parameter of the problem.

Equations of motion for minor body (asteroid) in canonical form:

$$\frac{d(L,G,H)}{dt} = -\frac{\partial \mathcal{K}}{\partial(l,g,h)}, \quad \frac{d(l,g,h)}{dt} = \frac{\partial \mathcal{K}}{\partial(L,G,H)}, \tag{28}$$

where L, G, H, l, g, h are the Delaunay variables (Murray and Dermott 2000). They can be expressed in terms of Keplerian elements a, e, i, Ω, ω as

$$L = \sqrt{(1-\mu)a}, \quad G = L\sqrt{1-e^2}, \quad H = G\cos i, \quad g = \omega, \quad h = \Omega.$$

The last variable l is the asteroid's mean anomaly.

Hamiltonian $\mathcal{K}$ in (28) is

$$\mathcal{K} = -\frac{(1-\mu)^2}{2L^2} - \mu R(L, G, H, l, g, h - \lambda'). \tag{29}$$

Here R is disturbing function in restricted circular three-body problem. Mean anomaly λ' appearing in (29) depends linearly on time: $\lambda' = t + \lambda'_0$. Therefore it is convenient to use variable $\tilde{h} = h - \lambda'$ instead of h, as it enables writing down the equations of motion in autonomous form as canonical equations with Hamiltonian

$$\tilde{\mathcal{K}} = \mathcal{K}(L, G, H, l, g, \tilde{h}) - H.$$

We introduce resonant angle $\bar{\varphi}$ using the canonical transformation $(L, G, H, l, g, \tilde{h}) \to (P_\varphi, P_g, P_h, \bar{\varphi}, \bar{g}, \bar{h})$ defined by generating function

$$S = (p+1)P_\varphi l + \left[P_h + p\left(P_\varphi - P_\varphi^*\right)\right]\tilde{h} + \left[P_g + (p+1)\left(P_\varphi - P_\varphi^*\right)\right]g,$$

where $P_\varphi^* = L_*/(p+1)$, while $L_* = \sqrt[3]{(p+1)/p}$ is the value of L corresponding to exact $p:(p+1)$ MMR in unperturbed problem ($\mu = 0$). The new variables are related to the old ones as follows:

$$L = \frac{\partial S}{\partial l} = (p+1)P_\varphi, \quad G = \frac{\partial S}{\partial g} = P_g + (p+1)\left(P_\varphi - P_\varphi^*\right),$$

$$H = \frac{\partial S}{\partial \tilde{h}} = P_h + p\left(P_\varphi - P_\varphi^*\right),$$

$$\bar{\varphi} = \frac{\partial S}{\partial P_\varphi} = (p+1)l + p\tilde{h} + (p+1)g, \quad \bar{g} = \frac{\partial S}{\partial P_g} = g, \quad \bar{h} = \frac{\partial S}{\partial P_h} = \tilde{h}.$$

The resonant angle can also be expressed in traditional form

$$\bar{\varphi} = (p+1)\lambda - p\lambda' - \Omega.$$

New Hamiltonian

$$\tilde{\mathcal{K}} = -\frac{(1-\mu)^2}{2(p+1)^2 P_\varphi^2} - \left[P_h + p(P_\varphi - P_\varphi^*)\right] - \mu R.$$

The resonant case we are interested in corresponds to region $\mathcal{R}$ of phase space, selected by the condition

$$\left|pn' - (p+1)n\right| \lesssim \mu^{1/2}.$$

Here $n' = 1$ and n are mean motions of planet and asteroid respectively. It is also true in $\mathcal{R}$ that

$$\left|P_\varphi - P_\varphi^*\right| \lesssim \mu^{1/2}. \tag{30}$$

In the resonant case, i.e. when the previous inequation holds, variables can be divided into *fast*, *semi-fast* and *slow*. Fast and semi-fast variables in $\mathcal{R}$ are $\bar{h}$ and $\bar{\varphi}$ respectively:

$$\frac{d\bar{h}}{dt} \sim 1, \quad \frac{d\bar{\varphi}}{dt} \sim \mu^{1/2}.$$

Slow variables, which vary with a rate of order μ, are P_φ, P_g, P_h, and $\bar{g}$.

To study secular effects the averaging over the fast variable $\bar{h}$ is performed, which results in equations of motion taking a canonical form with Hamiltonian

$$\bar{\mathcal{K}}(P_\varphi, P_g, P_h, \bar{\varphi}, \bar{g}) = \\ = \frac{1}{2\pi(p+1)} \int_0^{2\pi(p+1)} \tilde{\mathcal{K}}(L(P_\varphi), G(P_g, P_\varphi), H(P_h, P_\varphi), l(\bar{\varphi}, \bar{g}, \bar{h}), \bar{g}, \bar{h})\, d\bar{h},$$

where

$$l(\bar{\varphi},\bar{g},\bar{h}) = \frac{1}{k+1}\left[\bar{\varphi} - (k+1)\bar{g} - k\bar{h}\right].$$

After such averaging the fast variable $\bar{h}$ vanishes, and the term "fast" is exempted. Thus in the rest of the paper we adopt name *fast* for denoting variables, which vary with the rate $\mu^{1/2}$, instead of referring to them as semi-fast, when the distinction of three different time scales was needed.

Moreover, because there is no longer $\bar{h}$ in the Hamiltonian $\bar{\mathcal{K}}$, the conjugate momentum P_h is a constant in considered approximation and can be treated as a parameter of the problem. Thus $\bar{\mathcal{K}}$ is the Hamiltonian of a system with two degrees of freedom. Further instead of P_h we shall use parameter

$$\sigma = \sqrt{1 - \frac{P_h^2}{L_*^2}}.$$

Inequation $e \le \sigma$ defines region $\mathcal{S}$ in phase space, to which the motion of the system is bound by the Kozai-Lidov integral (Sidorenko et al. 2014).

Next standard step in analysis of system's dynamics in resonant region $\mathcal{R}$ is the scaling transformation (Arnold et al. 2006):

$$\bar{\tau} = \bar{\varepsilon}t, \quad \bar{\Phi} = (P_\varphi^* - P_\varphi)/\bar{\varepsilon}, \tag{31}$$

where $\bar{\varepsilon} = \mu^{1/2}$ is a new small parameter. Using variables (31), the equations of motion can be rewritten in a form of slow-fast system without loss of accuracy:

$$\begin{aligned} \frac{d\bar{\varphi}}{d\bar{\tau}} &= \chi\bar{\Phi}, \quad \frac{d\bar{\Phi}}{d\bar{\tau}} = -\frac{\partial\bar{W}}{\partial\bar{\varphi}}, \\ \frac{dP_g}{d\bar{\tau}} &= \bar{\varepsilon}\frac{\partial\bar{W}}{\partial\bar{g}}, \quad \frac{d\bar{g}}{d\bar{\tau}} = -\bar{\varepsilon}\frac{\partial\bar{W}}{\partial P_g}. \end{aligned} \tag{32}$$

Here

$$\chi = 3p^{4/3}(p+1)^{2/3},$$

$$\bar{W}(\bar{\varphi},\bar{g},P_g;\sigma) = \frac{1}{2\pi(k+1)}\int_0^{2\pi(k+1)} R\left(L_*, P_g, L_*\sqrt{1-\sigma^2}, l(\bar{\varphi},\bar{g},\bar{h}), \bar{g}, \bar{h}\right) d\bar{h}.$$

For $\sigma \ll 1$ the approximate expression for $\bar{W}(\bar{\varphi},\bar{g},P_g;\sigma)$ can be obtained as a series expansion (Murray and Dermott 2000):

$$\begin{aligned} \bar{W}(\bar{\varphi},\bar{g},P_g;\sigma) \approx W_0 + W_1 e\cos(\bar{\varphi}-\bar{g}) + \\ + e^2\left[W_{10} + W_{11}\cos 2(\bar{\varphi}-\bar{g})\right] + i^2\left[W_{20} + W_{21}\cos 2\bar{\varphi}\right], \end{aligned} \tag{33}$$

where

$$e^2 \approx 1 - \frac{P_g^2}{L_*^2}, \quad i^2 \approx 2\left(1 - \frac{P_h}{L_*\sqrt{1-e^2}}\right) \approx \sigma^2 - e^2. \tag{34}$$

Expressions (34) are obtained taking into account resonance condition (30), and that the values e and i are limited by $\sigma \ll 1$, leading to $e, i \ll 1$.

Coefficients W_0, W_1, W_{10}, W_{11}, W_{20}, W_{21} in (33) are calculated as follows:

$$\begin{aligned} &W_0 = \tfrac{\alpha}{2}b_{1/2}^{(0)}, \quad W_1 = \tfrac{\alpha}{2}\left[(2p+1)b_{1/2}^{(p)} + \alpha\tfrac{db_{1/2}^{(p)}}{d\alpha}\right] - \tfrac{\delta_{1p}}{2\alpha}, \\ &W_{10} = \tfrac{\alpha^2}{8}\left(2\tfrac{db_{1/2}^{(0)}}{d\alpha} + \alpha\tfrac{d^2b_{1/2}^{(0)}}{d\alpha^2}\right), \\ &W_{11} = \tfrac{\alpha}{8}\left(\left[2 - 14(p+1) + 16(p+1)^2\right]b_{1/2}^{(2p)} + \alpha\left[8(p+1)-2\right]\tfrac{db_{1/2}^{(2p)}}{d\alpha} + \alpha^2\tfrac{d^2b_{1/2}^{(2p)}}{d\alpha^2}\right), \\ &W_{20} = -W_{10}, \quad W_{21} = \tfrac{\alpha^2}{8}b_{3/2}^{(2p+1)}. \end{aligned} \tag{35}$$

Here $\alpha = (p/(p+1))^{2/3}$, δ_{mn} is the Kronecker delta, and $b_{1/2}^{(n)}(\alpha)$, $b_{3/2}^{(n)}(\alpha)$ are Laplace coefficients. Numerical values of coefficients (35) for several resonances are gathered in Table 1.

Table 1 Numerical values of coefficients in series expansion of averaged disturbing function

	$p=1$	$p=2$	$p=3$	$p=4$	$p=5$
W_0	0.7120	0.9381	1.0767	1.1760	1.2531
W_1	0.2699	1.8957	2.7103	3.5192	4.3257
W_{10}	0.2442	0.8798	1.8815	3.2449	4.9686
W_{11}	2.2640	6.3052	12.260	20.133	29.923
W_{21}	0.1291	0.4375	0.9160	1.5640	2.3814

Out of the whole region $\mathcal{S}$ we are interested in the part with small eccentricities. Thus we further assume $e/\sigma \lesssim \sigma$, which leads to $e \lesssim \sigma^2$. Taking into account (34) we can write down expression for averaged disturbing function up to the terms of order σ^2:

$$\bar{W}(\bar{\varphi}, \bar{g}, P_g; \sigma) \approx W_0 + W_1 e \cos(\bar{\varphi} - \bar{g}) + \sigma^2 \left[W_{20} + W_{21} \cos 2\bar{\varphi}\right].$$

By introducing the variables

$$\bar{x} = \sqrt{2(L_* - P_g)} \cos \bar{g}, \quad \bar{y} = -\sqrt{2(L_* - P_g)} \sin \bar{g},$$

the equations of motion (32) can be reduced to a Hamiltonian form

$$\begin{aligned} \frac{d\bar{\varphi}}{d\bar{\tau}} &= \frac{\partial \bar{\Xi}}{\partial \bar{\Phi}}, \quad \frac{d\bar{\Phi}}{d\bar{\tau}} = -\frac{\partial \bar{\Xi}}{\partial \bar{\varphi}}, \\ \frac{d\bar{x}}{d\bar{\tau}} &= \bar{\varepsilon} \frac{\partial \bar{\Xi}}{\partial \bar{y}}, \quad \frac{d\bar{y}}{d\bar{\tau}} = -\bar{\varepsilon} \frac{\partial \bar{\Xi}}{\partial \bar{x}} \end{aligned}$$

with the Hamiltonian

$$\bar{\Xi} = \frac{\chi \bar{\Phi}^2}{2} + \frac{W_1}{\sqrt{L_*}} \cos \bar{\varphi} \cdot \bar{x} - \frac{W_1}{\sqrt{L_*}} \sin \bar{\varphi} \cdot \bar{y} + \sigma^2 W_{21} \cos 2\bar{\varphi}.$$

The final rescaling of variables

$$\begin{aligned} \varphi &= -\bar{\varphi}, \quad \Phi = -\sqrt{\frac{\chi}{\sigma^2 W_{21}}} \bar{\Phi}, \\ x &= \frac{W_1}{\sigma^2 W_{21} \sqrt{L_*}} \bar{x}, \quad y = \frac{W_1}{\sigma^2 W_{21} \sqrt{L_*}} \bar{y}, \\ \tau &= \sigma \sqrt{\chi W_{21}} \bar{\tau}, \quad \varepsilon = \frac{{W_1}^2}{\chi^{1/2} L_* \sigma^3 W_{21}^{3/2}} \bar{\varepsilon} \end{aligned} \tag{36}$$

results in the model system (1)–(2).

Appendix B: Analytical expressions for integrals, emerging during the averaging over fast subsystem's period

Right-hand side parts of evolution equations (4), as well as adiabatic invariant formula (22), can be expressed in terms of integrals

$$I_{k,r} = \int_{\lambda_*}^{\lambda^*} \frac{\lambda^r d\lambda}{(\lambda^2+1)^k \sqrt{\pm(\lambda - a_1)(\lambda - a_2)(\lambda - a_3)(\lambda - a_4)}},$$

where $k = 0, 1, 2$; $r = 0, 1$, and integration limits λ_*, λ^* can be either real numbers or $\pm\infty$. These integrals can be reduced to the linear combinations of elliptic integrals of the first, the second and the third kind:

$$\begin{array}{l} I_{0,0} = c_{0,0}K(k), \\ I_{1,0} = c_{1,1}K(k) + c_{1,3}\Pi\left(h,k\right) + \bar{c}_{1,3}\Pi\left(\bar{h},k\right), \\ I_{1,1} = g_{1,1}K(k) + g_{1,3}\Pi\left(h,k\right) + \bar{g}_{1,3}\Pi\left(\bar{h},k\right), \\ I_{2,0} = \frac{1}{2}I_{1,0} + c_{2,1}K(k) + c_{2,2}E(k) + c_{2,3}\Pi\left(h,k\right) + \bar{c}_{2,3}\Pi\left(\bar{h},k\right), \\ I_{2,1} = g_{2,1}K(k) + g_{2,2}E(k) + g_{2,3}\Pi\left(h,k\right) + \bar{g}_{2,3}\Pi\left(\bar{h},k\right). \end{array} \tag{37}$$

Further the formulae for coefficients $c_{m,l}$, $g_{m,l}$, moduli k and parameters h are gathered for all necessary cases.

The case $a_j \in \mathbb{R}^1$ $(j = \overline{1,4})$

We will further assume, that a_j are numbered in ascending order:

$$a_1 < a_2 < a_3 < a_4.$$

Four different instances should be considered:

A. Integration over (a_1, a_2);
B. Integration over (a_2, a_3);
C. Integration over (a_3, a_4);
D. Integration over $(-\infty, a_1)\bigcup(a_4, +\infty)$.

Instance A

Here $\lambda_* = a_1$ and $\lambda^* = a_2$. We shall also use the following auxiliary parameters:

$$A_0 = \frac{2}{\sqrt{(a_4-a_2)(a_3-a_1)}}, \quad C_0 = \frac{1}{a_2-i}, \quad \alpha^2 = \frac{a_2-a_1}{a_3-a_1}, \quad \alpha_1^2 = \frac{(a_2-a_1)(i-a_3)}{(a_3-a_1)(i-a_2)}.$$

The value of elliptic integrals' modulus in (37):

$$k = \sqrt{\frac{(a_4-a_3)(a_2-a_1)}{(a_4-a_2)(a_3-a_1)}},$$

and parameter $h = \alpha_1^2$.

In order to find coefficients in (37), we considered such linear combinations of $I_{k,r}$, that are reduced to integral (253.39) from (Byrd and Friedman 1954):

$$\begin{array}{l} I_{1,1} + iI_{1,0} = \int\limits_{a_1}^{a_2} \frac{d\lambda}{(\lambda-i)\sqrt{-(\lambda-a_1)(\lambda-a_2)(\lambda-a_3)(\lambda-a_4)}}, \\ I_{2,0} - iI_{2,1} - \frac{1}{2}I_{1,0} = -\frac{1}{2}\int\limits_{a_1}^{a_2} \frac{d\lambda}{(\lambda-i)^2\sqrt{-(\lambda-a_1)(\lambda-a_2)(\lambda-a_3)(\lambda-a_4)}}. \end{array} \tag{38}$$

After some simple calculations, one can find:

$$\begin{array}{l} g_{1,1} = \operatorname{Re} C_1, \quad c_{1,1} = \operatorname{Im} C_1, \quad C_1 = \frac{A_0 C_0 \alpha^2}{\alpha_1^2}, \\ g_{1,3} = \frac{A_0 C_0}{2}\left(1 - \frac{\alpha^2}{\alpha_1^2}\right), \quad c_{1,3} = -ig_{1,3}, \\ c_{2,1} = -\operatorname{Re} C_2, \quad g_{2,1} = \operatorname{Im} C_2, \quad C_2 = \frac{A_0 C_0^2}{2\alpha_1^4}\left[\alpha^4 + \frac{(\alpha_1^2-\alpha^2)^2}{2(\alpha_1^2-1)}\right], \\ c_{2,2} = -\operatorname{Re} C_3, \quad g_{2,2} = \operatorname{Im} C_3, \quad C_3 = \frac{A_0 C_0^2 (\alpha_1^2-\alpha^2)^2}{4\alpha_1^2(\alpha_1^2-1)(k^2-\alpha_1^2)}, \\ c_{2,3} = -\frac{A_0 C_0^2(\alpha_1^2-\alpha^2)}{4\alpha_1^4}\left[2\alpha^2 + \frac{(2\alpha_1^2k^2+2\alpha_1^2-\alpha_1^4-3k^2)(\alpha_1^2-\alpha^2)}{2(\alpha_1^2-1)(k^2-\alpha_1^2)}\right], \\ g_{2,3} = ic_{2,3}. \end{array} \tag{39}$$

Using (253.00) from Byrd and Friedman (1954) we also obtain:

$$c_{0,0} = A_0. \tag{40}$$

Instance B

For integrals over the interval (a_2, a_3) the only difference is the parameters α^2, α_1^2 and modulus k. Thus in (39) the values

$$\alpha^2 = \frac{a_3 - a_2}{a_3 - a_1}, \quad \alpha_1^2 = \frac{(a_3 - a_2)(i - a_1)}{(a_3 - a_1)(i - a_2)}, \quad k = \sqrt{\frac{(a_3 - a_2)(a_4 - a_1)}{(a_4 - a_2)(a_3 - a_1)}}$$

should be used.

Instance C

For integrals over the interval (a_3, a_4) in (39):

$$C_0 = \frac{1}{a_3 - i}, \quad \alpha^2 = \frac{a_4 - a_3}{a_4 - a_2}, \quad \alpha_1^2 = \frac{(a_4 - a_3)(i - a_2)}{(a_4 - a_2)(i - a_3)}.$$

The modulus k and parameter A_0 are the same as for interval (a_1, a_2).

Note: The equality of k and $c_{0,0}$ in instances A and C means, that when the potential (2) has two minima, the periods of librations T about them on the same energy level are equal. This also holds true for local minima corresponding to instances B and D, as the substitution $\lambda = \tan[(\varphi - \tilde{\varphi})/2]$ always allows to get rid of semi-infinite intervals of integration. Moreover, the averaged values of cos in (18) are also the same for librations around two local minima. The averaged values of sin in (18) for librations about two local minima differ by π, and values of adiabatic invariant (22) differ by $y/\sqrt{2}$.

Instance D

For integrals over two semi-infinite intervals the values of parameters in (39) are

$$C_0 = \frac{1}{a_4 - i}, \quad \alpha^2 = \frac{a_4 - a_1}{a_3 - a_1}, \quad \alpha_1^2 = \frac{(a_4 - a_1)(i - a_3)}{(a_3 - a_1)(i - a_4)}.$$

The modulus k is the same as for integration over (a_2, a_3), and A_0 is the same as for (a_1, a_2).

The case $a_1, a_2 \in \mathbb{R}^1$ $(a_1 < a_2)$, $a_3, a_4 \in \mathbb{C}^1$ $(a_3 = \bar{a}_4)$

Here there are only two instances:

A. Integration over (a_1, a_2);
B. Integration over $(-\infty, a_1) \bigcup (a_2, +\infty)$.

Instance A

Here the following auxiliary parameters in expressions for $c_{m,l}$ and $g_{m,l}$ will be used:

$$\alpha = \frac{(a_1 A_2 - a_2 A_1) - (A_2 - A_1)i}{(a_1 A_2 + a_2 A_1) - (A_2 + A_1)i}, \quad \alpha_1 = \frac{A_2 - A_1}{A_2 + A_1},$$

$$C_0 = \frac{A_1 + A_2}{(A_2 a_1 - A_1 a_2) - (A_2 - A_1)i},$$

where

$$A_1 = \sqrt{(a_1 - a_0)^2 + b_0^2}, \quad A_2 = \sqrt{(a_2 - a_0)^2 + b_0^2}, \quad A_0 = 1/\sqrt{A_1 A_2},$$
$$a_0 = \operatorname{Re} a_3 = \operatorname{Re} a_4, \quad b_0 = \operatorname{Im} a_3 = -\operatorname{Im} a_4.$$

Using (38) and formulae (259.04), (341.01)–(341.04)[2] from (Byrd and Friedman 1954), we obtain

$$\begin{aligned}
&c_{0,0} = 2A_0, \quad g_{1,1} = \operatorname{Re} C_1, \quad c_{1,1} = \operatorname{Im} C_1, \quad C_1 = 2A_0C_0\alpha_1,\\
&c_{1,3} = -\tfrac{i(\alpha-\alpha_1)}{(1-\alpha^2)}A_0C_0, \quad g_{1,3} = ic_{1,3},\\
&c_{2,1} = -\operatorname{Re} C_2, \quad g_{2,1} = \operatorname{Im} C_2, \quad C_2 = A_0C_0^2\left[\alpha_1^2 + \tfrac{(\alpha-\alpha_1)^2}{\alpha^2-1}\right],\\
&c_{2,2} = -\operatorname{Re} C_3, \quad g_{2,2} = \operatorname{Im} C_3, \quad C_3 = \tfrac{A_0C_0^2\alpha^2(\alpha-\alpha_1)^2}{(1-\alpha^2)(k^2+\alpha^2k'^2)},\\
&c_{2,3} = \tfrac{A_0C_0^2}{2}\tfrac{(\alpha-\alpha_1)}{(\alpha^2-1)}\left[2\alpha_1 + \tfrac{(\alpha-\alpha_1)\left[\alpha^2(2k-1)-2k^2\right]}{(\alpha^2-1)(k^2+\alpha^2k'^2)}\right], \quad g_{2,3} = ic_{2,3}.
\end{aligned} \tag{41}$$

Modulus and parameter of elliptic integrals are calculated as follows:

$$k = \sqrt{\frac{(a_2-a_1)^2 - (A_2-A_1)^2}{4A_1A_2}}, \quad h = \frac{\alpha^2}{\alpha^2-1}.$$

Instance B

Expressions (41) stay the same. Auxiliary parameters are

$$\alpha = \frac{(a_2A_1 + a_1A_2) - (A_2+A_1)i}{(a_2A_1 - a_1A_2) + (A_2-A_1)i}, \quad \alpha_1 = \frac{A_2+A_1}{A_1-A_2},$$

$$C_0 = \frac{A_1-A_2}{(A_2a_1 + A_1a_2) - (A_2+A_1)i}.$$

The modulus k of elliptic integrals is also different:

$$k = \sqrt{\frac{(A_2+A_1)^2 - (a_2-a_1)^2}{4A_1A_2}}.$$

The case $a_j \in \mathbb{C}^1$ $(j = \overline{1,4})$

Let us denote real parts of roots a_j as $p_{1,2}$, and imaginary parts as $b_{1,2}$:

$$a_{1,2} = p_1 \pm b_1, \quad a_{3,4} = p_2 \pm b_2.$$

Without loss of generality let us assume, that $p_1 < p_2$, $b_1 > 0$, and $b_2 > 0$ (if $p_1 = p_2$, then also $b_1 < b_2$). In expressions for $c_{m,l}$ and $g_{m,l}$ the following auxiliary parameters will be used

$$A_1 = \sqrt{(p_2-p_1)^2 + (b_2-b_1)^2}, \quad A_2 = \sqrt{(p_2-p_1)^2 + (b_2+b_1)^2}, \quad A_0 = 2/(A_1+A_2),$$

$$g_1 = \sqrt{\frac{4b_1^2 - (A_2-A_1)^2}{(A_2+A_1)^2 - 4b_1^2}}, \quad \alpha = \frac{b_1 + g_1(p_1-i)}{p_1 - b_1g_1 - i}, \quad C_0 = \frac{1}{b_1 + g_1(p_1-i)}.$$

Similar to previous case we find:

$$\begin{aligned}
&c_{0,0} = 2A_0, \quad c_{1,1} = \operatorname{Im} C_1, \quad g_{1,1} = \operatorname{Re} C_1, \quad C_1 = \tfrac{2\alpha(1+g_1\alpha)}{1+\alpha^2}A_0C_0,\\
&g_{1,3} = \tfrac{\alpha^2(\alpha-g_1)A_0C_0}{1+\alpha^2}, \quad c_{1,3} = -ig_{1,3}, \quad c_{2,1} = -\operatorname{Re} C_2, \quad g_{2,1} = \operatorname{Im} C_2,\\
&C_2 = A_0C_0^2\left[g_1^2 + \tfrac{2g_1(\alpha-g_1)}{1+\alpha^2} + \tfrac{(\alpha-g_1)^2}{(1+\alpha^2)(\alpha^2+k'^2)}\left(\tfrac{2k'^2+2\alpha^2-\alpha^2k^2}{1+\alpha^2} - k'^2\right)\right],\\
&c_{2,2} = \operatorname{Re} C_3, \quad g_{2,2} = -\operatorname{Im} C_3, \quad C_3 = \tfrac{A_0C_0^2(\alpha-g_1)^2\alpha^2}{(\alpha^2+1)(\alpha^2+k'^2)},\\
&c_{2,3} = -\tfrac{A_0C_0^2}{2}\tfrac{(\alpha-g_1)\alpha^2}{(\alpha^2+1)}\left[2g_1 + \tfrac{(\alpha-g_1)(2k'^2+2\alpha^2-\alpha^2k^2)}{(\alpha^2+1)(\alpha^2+k'^2)}\right], \quad g_{2,3} = ic_{2,3}.
\end{aligned}$$

Modulus and parameter of elliptic integrals:

$$k = \frac{2\sqrt{A_1A_2}}{A_1+A_2}, \quad h = \alpha^2 + 1.$$

[2] It should be noted, that (259.04) in (Byrd and Friedman 1954) contain a typo – the multiplier g (in authors' notation) is missing.

Acknowledgements The work was supported by the Presidium of the Russian Academy of Sciences (Program 28 "Space: investigations of the fundamental processes and their interrelationships"). We are grateful to A.I.Neishtadt, A.Correia, A.Morbidelli and J.Wisdom for useful discussions. We would also like to thank D.A.Pritykin for proof-reading the manuscript.

References

Arnold V, Kozlov V, Neishtadt A (2006) Mathematical Aspects of Classical and Celestial Mechanics, 3rd edn. Springer, New York

Arnold VI (1963) Small denominators and problems of stability of motion in classical and celestial mechanics. Russian Mathematical Surveys 18(6(114)):91–192

Artemyev AV, Neishtadt AI, Zeleny LM (2013) Ion motion in the current sheet with sheared magnetic field – Part 1: Quasi-adiabatic theory. Nonlin Processes Geophys 20:163–178

Batkhin AB (2012) Application of the method of asymptotic solution to one multi-parameter problem. in: Gerdt V.P., Koepf W., Mayr E.W., Vorozhtsov E.V. (eds) Computer Algebra in Scientific Computing. CASC 2012. Springer, Berlin, Heidelberg, Lecture Notes in Computer Science, vol 7442, pp 22–33

Beaugé C (1994) Asymmetric liberations in exterior resonances. Celestial Mechanics and Dynamical Astronomy 60(2):225–248

Broz M, Vokrouhlicky D (2008) Asteroid families in the first-order resonance with Jupiter. MNRAS 390:715–732

Byrd PF, Friedman MD (1954) Handbook of elliptic integrals for engineers and physicists. Springer-Verlag, Berlin-Göttingen-Heidelberg

Chambers JE (1999) A hybrid symplectic integrator that permits close encounters between massive bodies. Monthly Notices of the Royal Astronomical Society 304(4):793–799

Gallardo T (2018) Resonances in the asteroid and trans-Neptunian belts: A brief review. Planetary and Space Science

Gerasimov I, Mushailov B (1990) Evolution of asteroid orbits in the case of first-order commensurability. Exterior problem. Sov Astron 34:440–444

Giffen R (1973) A Study of Commensurable Motion in the Asteroid Belt. Astronomy and Astrophysics 23:387–403

Henrard J (1996) A note concerning the 2:1 and the 3:2 resonances in the asteroid belt. Celestial Mechanics and Dynamical Astronomy 64:107–114

Henrard J, Lamaitre A (1983) A Second Fundamental Model for Resonance. Celestial Mechanics 30:197–218

Holmes P (1990) Poincare, celestial mechanics, dynamical systems theory and "chaos". Phys Reports 193:137–163

Jancart S, Lemaitre A, Istace A (2002) Second fundamental model of resonance with asymmetric equilibria. Celestial Mechanics and Dynamical Astronomy 84:197–221

Lang HA, Stevens DF (1960) On the evaluation of certain complex elliptic integrals. Mathematics of Computation 14:195–199

Lemaitre A, Henrard J (1990) On the origin of chaotic behavior in the 2/1 Kirkwood gap. Icarus 83:391–403

Li J, Zhou LY, Sun YS (2014a) A study of the high-inclination population in the Kuiper belt – I. The plutinos. MNRAS 437:215–226

Li J, Zhou LY, Sun YS (2014b) A study of the high-inclination population in the Kuiper belt - II. The twotinos. MNRAS 443:1346–1375

Lissauer J (1999) Chaotic motion in the Solar system. Reviews of Modern Physics 71:835–845

Morbidelli A (2002) Modern celestial mechanics. Aspects of Solar system dynamics. Taylor & Francis, London–New York

Murray CD, Dermott SF (2000) Solar System Dynamics. Cambridge University Press, Cambridge

Neishtadt AI (1987a) Jumps of the adiabatic invariant on crossing a separatrix and the origin of the Kirkwood gap 3:1. Doklady Physics 32:571–573

Neishtadt AI (1987b) Jumps of the adiabatic invariant on crossing a separatrix in systems with two degrees of freedom. PMM USSR 51:586–592

Neishtadt AI, Sidorenko VV (2004) Wisdom system: Dynamics in the adiabatic approximation. Celestial Mech Dyn Astr 90:307–330

Nesvorny D, Roig F (2000) Mean motion resonances in the trans-Neptunian region. I. The 2:3 resonance with Neptune. Icarus 148:282–300

Nesvorny D, Roig F (2001) Mean motion resonances in the trans-Neptunian region. II. The 1:2, 3:4 and weaker resonances. Icarus 150:104–123

Nesvorny D, Ferraz-Mello S, Holman M, Morbidelli A (2002) Regular and chaotic dynamics in the mean-motion resonances: implications for the structure and evolution of the asteroid belt. In: Bottke W, Cellino A, Paolicchi P, Binzel R (eds) Asteroids III, University of Arizona Press, Tucson, pp 379–394

Sessin W, Ferraz-Mello S (1984) Motion of two planets with periods commensurable in the ratio 2:1. Solutions of the Hori auxiliary system. Celestial Mechanics and Dynamical Astronomy 32:307–332

Sidorenko VV (2006) Evolution of asteroid orbits at resonance 3:1 of their mean motions with Jupiter (planar problem). Cosm Res 44:440–455

Sidorenko VV (2018) Dynamics of "jumping" Trojans: a perturbative treatment. Celestial Mechanics and Dynamical Astronomy (in press)

Sidorenko VV, Neishtadt AI, Artemyev AV, Zelenyi LM (2014) Quasi-satellite orbits in the general context of dynamics in the 1:1 mean motion resonance. Perturbative treatment. Celestial Mechanics and Dynamical Astronomy 120(2):131–162

Tennyson JL, Cary JR, Escande DF (1986) Change of the adiabatic invariant due to separatrix crossing. Phys Rev Lett 56:2117–2120

Winter O, Murray C (1997a) Resonance and chaos. I. First-order interior resonances. Astron Astrophys 319:290–304

Winter O, Murray C (1997b) Resonance and chaos. II. Exterior resonances and asymmetric libration. Astron Astrophys 328:399–408

Wisdom J (1985) A perturbative treatment of motion near the 3/1 commensurability. Icarus 63:272–289

Wisdom J (1986) Canonical solution of the two critical argument problem. Celestial Mechanics and Dynamical Astronomy 38:175–180

Wisdom J (1987) Urey prize lecture: chaotic dynamics in the Solar system. Icarus 72:241–275

Wisdom J, Sussman GJ (1988) Numerical evidence that the motion of Pluto is chaotic. Bulletin of the American Astronomical Society 20:901